

# Gravitational and distributed heating effects of a cD galaxy on the hydrodynamical structure of its host cluster

Curtis J. Saxton<sup>1\*</sup> & Kinwah Wu<sup>1</sup>

<sup>1</sup>*Mullard Space Science Laboratory, University College London, Holmbury St Mary, Surrey RH5 6NT, UK*

Accepted 2013 November 7. Received 2013 November 5; in original form 2012 December 27

## ABSTRACT

We investigate the effects of a cD galaxy’s gravity and AGN heating of the host galaxy cluster. We consider a standard prescription for the hydrodynamics, with the structures determined by mass continuity, momentum and energy conservation equations in spherical symmetry. The cluster comprises a dark matter halo (DM) and ionized X-ray emitting intracluster gas (ICM), which jointly determine the gravitational potential. The cD galaxy is an additive gravitational potential component. The DM assumes a polytropic equation of state (determined by its microphysics), which could be non-radiative self-interacting particles or more exotically interacting particles. The AGN provides distributed heating, counteracting radiative cooling. Stationary density and velocity dispersion profiles are obtained by numerically integrating the hydrodynamic equations with appropriate boundary conditions. The minimum gas temperature in the cluster core is higher when a cD galaxy is present than when it is absent. The solutions also yield a point-like mass concentration exceeding a minimum mass: presumably the AGN’s supermassive black hole (SMBH). Consistency with observed SMBH masses constrains the possible DM equations of state. The constraints are looser when a cD galaxy is present. Distributed (AGN) heating alters cluster global properties, and also reduces the lower limits for the central point-mass, for the preferred DM models in which the dark particles have greater heat capacity than point particles. Eluding these constraints would require dominant non-spherical or anisotropic effects (e.g. bulk rotation, non-radial streaming, asymmetric lumps or a strong magnetic field).

**Key words:** hydrodynamics — dark matter — galaxies: active — galaxies: clusters: general — galaxies: clusters: intracluster medium — galaxies: elliptical and lenticular, cD — dark matter

## 1 INTRODUCTION

In galaxy clusters, most of the visible matter exists as the X-ray emitting gas of the intracluster medium (ICM), which is outweighed by the dark matter halo (DM) inferred to bind the system together. It has long been recognized that gas cooling in undisturbed clusters must weaken central pressure support, leading to gas inflow from the outskirts. In the conventional ‘cooling flow’ models (e.g. Fabian & Nulsen 1977; Cowie & Binney 1977; Stewart et al. 1984; Nulsen 1986; Johnstone et al. 1992) runaway inflows would deposit multiphase cold gas throughout a 0.3 Mpc cool core at rates of  $10^1$ – $10^3 m_{\odot} \text{ yr}^{-1}$ . Observationally, these cold condensates do not occur in the predicted amounts, and the ICM appears single-phase (e.g. Ikebe et al. 1997; Böhringer et al. 2001; David et al. 2001;

Kaastra et al. 2001; Tamura et al. 2001; Peterson et al. 2001; Molendi & Pizzolato 2001; Matsushita et al. 2002; Donahue & Voit 2004; Peterson & Fabian 2006). In the cool cores of clusters and groups, the gas temperatures are observed to drop, but rarely (Centaurus: Sanders et al. 2008) more than a factor  $\sim 2$ – $5$  below the peak temperature (e.g. Sakelliou et al. 2002; Ettori et al. 2002; Johnstone et al. 2002; Peterson et al. 2003; Voigt & Fabian 2004; Xue, Böhringer & Matsushita 2004; Bauer et al. 2005; Zhang et al. 2006; Reiprich et al. 2009; O’Sullivan et al. 2011; Moretti et al. 2011; Bulbul et al. 2012). In some cool cores, the temperature actually rises at small radii around a central galaxy (O’Sullivan et al. 2007; Sun et al. 2009).

To remedy this runaway cooling-induced inflow problem, non-gravitational heating, usually by active galaxies (AGN), was invoked to staunch the inflows (see e.g. reviews by Peterson & Fabian 2006; McNamara & Nulsen 2007). Yet it is questionable whether the heating can be suf-

\* E-mail: cjs2@mssl.ucl.ac.uk (CJS); kw@mssl.ucl.ac.uk (KW)

ficiently well distributed to attain finely balanced ‘feedback’ that actively controls clusters of all types. Although bubbles blown by active galaxies should contain enough heat for clusters in general (e.g. Churazov et al. 2001; Birzan et al. 2004; Dunn, Fabian & Taylor 2005), it is uncertain how well the hot plasma in the bubble would mix with the ICM (e.g. Dursi 2007). It is also unknown whether the compression of the ICM by bubble-generated shocks actually exacerbates or halts the cooling (e.g. Brighenti & Mathews 2003; Conroy & Ostriker 2008).

The nature of dark matter remains speculative and contentious. On the one hand,  $N$ -body simulations reproduce large-scale cosmic structures resembling those observed; on the other hand, simulations also produce results inconsistent with various observations. If the dark matter is assumed to experience only gravitation, the abundance of luminous substructure is overpredicted, for Milky Way satellites (e.g. Klypin et al. 1999; Moore et al. 1999), for galaxies in some groups (D’Onghia & Lake 2004), in cosmic voids (Tikhonov & Klypin 2009; Peebles & Nusser 2010) and at higher redshifts (Miller et al. 2013). More problematically, the largest observed satellite galaxies are less massive than the corresponding predicted subhaloes (Boylan-Kolchin, Bullock & Kaplinghat 2011, 2012). Collisionless DM models also predict singular central density *cusps* of dark matter in galaxies and clusters (Dubinski & Carlberg 1991; Navarro, Frenk & White 1996; Navarro et al. 2004; Merritt et al. 2005). To date, zero galaxies have unambiguously proven dark matter cusps. Instead, the evidence from diverse galaxy types either strongly requires, favours or allows dark matter *cores* of nearly uniform density (e.g. Flores & Primack 1994; Moore 1994; Burkert 1995; Salucci & Burkert 2000; Kelson et al. 2002; Kleyna et al. 2003; Goerdt et al. 2006; Gentile et al. 2004; de Blok 2005; Thomas et al. 2005; Kuzio de Naray et al. 2006; Gilmore et al. 2007; Weijmans et al. 2008; Oh et al. 2008; Nagino & Matsushita 2009; Inoue 2009; de Blok 2010; Pu et al. 2010; Murphy, Gebhardt & Adams 2011; Memola, Salucci & Babić 2011; Walker & Peñarrubia 2011; Jardel & Gebhardt 2012; Amorisco & Evans 2012; Agnello & Evans 2012). These imply that dark matter is not as simple as previously thought. It could well self-interact (i.e. self-interacting dark matter, SIDM), with the soft central cores emerging universally due to dark pressure support (e.g. Spergel & Steinhardt 2000; Firmani et al. 2000; Ahn & Shapiro 2005; Ackerman et al. 2009; Loeb & Weiner 2011; Vogelsberger, Zavala & Loeb 2012; Peter et al. 2013; Rocha et al. 2013).

An alternative remedy to rectify the cusp problem is the injection of mechanical energy into the halo. Through a ‘feedback’ mechanism that invokes supernovae and stellar wind outflows, the cusps are shaken flat (e.g. Navarro, Eke & Frenk 1996; Binney, Gerhard & Silk 2001). With ad hoc supernova recipes, this seems to work in some simulations of gassy dwarf galaxies (e.g. Mashchenko, Couchman & Wadsley 2006; Governato et al. 2010), but may be energetically impossible for DM-dominated dwarf spheroidals (Peñarrubia et al. 2012; Garrison-Kimmel et al. 2013). A total blowout of the baryons is still insufficient to erase cusps in a larger galactic disc (Gnedin & Zhao 2002). Nevertheless, the use of black-box recipes for subgrid stellar physics is computa-

tionally convenient, as the assumption of collisionless dark matter is retained. Sellwood (2009) reviews other baryonic mechanisms speculated to destroy dark cusps at galaxy scales. Similar energy-injection theories propose that the cusps of elliptical galaxies were erased by AGN feedback (Peirani, Kay & Silk 2008).

At cluster scales the observational evidence about the nature of dark matter is less settled than for galaxies. At least some X-ray, kinematic and gravitational lensing studies of clusters require or allow DM cores (Sand, Treu & Ellis 2002; Sand et al. 2008; Ettori et al. 2002; Halkola, Seitz & Pannella 2006; Halkola et al. 2008; Voigt & Fabian 2006; Rzepecki et al. 2007; Newman et al. 2009; Zitrin & Broadhurst 2009; Richtler et al. 2011), while others allow cuspy models (Athreya et al. 2002; Buote & Lewis 2004; Pointecouteau, Arnaud & Pratt 2005; Gavazzi 2005; Diego et al. 2005; Vikhlinin et al. 2006; Saha & Read 2009; Richard et al. 2009). Inclusion of information from the inner 100 or 30 kpc radii (especially stellar kinematics) tends to favour a core rather than cusp (e.g. Gavazzi 2005; Sand et al. 2008). It is sometimes claimed that asymmetric clusters are mergers (capable of disproving DM collisionality) but the evidence revolves around assumed motions and projected geometries of a handful of special objects. A particular ‘Bullet Cluster’, studied in X-rays and gravitational lensing, has been interpreted as a head-on merger with interpenetrating, non-interacting haloes (1E0657–56: Clowe et al. 2006; Randall et al. 2008), but since ICM shocks have not affected star formation as expected (Chung et al. 2009) a different story may be necessary. Another merger taken at face value (Abell 520) implies that dark matter behaves like gas, concentrated and separated from the collisionless galaxies (Mahdavi et al. 2007; Jee et al. 2012). Williams & Saha (2011) have investigated a gravitational lensing cluster (Abell 3827) in which the haloes of the innermost elliptical galaxies appear displaced from the stars, perhaps due to drag forces in the cluster halo.

The feedback recipes for eliminating cusps and staunching cooling flows could be elaborated for decades indecisively. It is therefore worthwhile to study alternative theories that produce the required structures inexorably. Our cluster model (Saxton & Wu 2008) revisits the cooling-induced inflow scenario in a more complete and consistent implementation, to reassess the natural behaviour of gas in a quiescent halo. We consider versions of halo physics (including SIDM) which produce DM cores naturally. Given a sensible radius and total cluster mass, we infer constraints on the DM parameters and the central object of the cluster. A favoured domain of DM thermal microphysics yields cores of realistic size ( $\sim 10^1$ – $10^2$  kpc). All stationary solutions of our model have non-zero gas temperatures and possess a central point-mass exceeding some minimum. Requiring consistency with the masses of observed black holes (e.g. Houghton et al. 2006; Inada et al. 2008; Cappellari et al. 2009; Gebhardt et al. 2011; McConnell et al. 2011, 2012) implies joint constraints on the dark matter physics and gas inflow rate. The tightest constraints on the continuity of the gas inflow occur at kpc radii, suggesting that this is the natural site for cold gas dropout (and star formation) during external disturbances. For the favoured DM models, it was also found that an inner portion of the dark halo teeters on the brink of gravitational collapse. The dark mass involved is

consistent with observed supermassive black holes (SMBH), hinting that these objects could feed non-radiatively in ‘dark gulping’ events.

This modelling omitted the stellar mass distribution of the cD galaxy that should realistically reside at the centre of an inflow of cooling gas, and surrounding the black hole. Stellar density is significant compared to dark matter within the half-light radii of elliptical galaxies (e.g. Loewenstein & White 1999; Kronawitter et al. 2000; Ferreras, Saha & Williams 2005; Thomas et al. 2007; Bolton et al. 2008; Saxton & Ferreras 2010; Norris et al. 2012). In this work, we introduce such a galaxy, and determine how it modifies the structure of the cluster’s gas inflow and dark halo. In particular, we investigate how the presence of a cD galaxy would affect the temperature floor of the ICM gas.

We also consider how AGN heating could affect cluster properties. To be effective, AGN power needs to be isotropically deposited in the cool core. Jet effects are directional (Vernaleo & Reynolds 2006) but they may be a feasible heating process if the jet axis slews and realigns widely enough between active episodes (Babul, Sharma & Reynolds 2013). These conditions are conceivable: some observed pairs of giant radio lobes suggest large angular slews between outbursts  $\lesssim 100$  Myr apart (e.g. Dunn, Fabian & Sanders 2006), while a blazar-like tidal disruption jet may precess and nutate through smaller angles on weekly time-scales (e.g. Sw J1644+57; Saxton et al. 2012). Streaming cosmic rays could provide a more innately isotropic heating process than jets (e.g. Fujita & Ohira 2011). In this paper we optimistically *assume* isotropic heating and consider various forms of radially distributed AGN power. We compare cases where the cD galaxy is active or inactive.

The paper is organized as follows: Section 2 describes the hydrodynamical formulation and the ingredients of the cluster model; in Section 3, we show the results of our calculations; Section 4 is a discussion; and §5 presents a brief summary of our findings.

## 2 HYDRODYNAMICAL STRUCTURE

### 2.1 Constituents

We consider spherical galaxy clusters consisting of two free, coterminous mass components (subscripted  $i = 1, 2$ ), interacting only via their shared gravitational potential (following Saxton & Wu 2008). The first component is the intra-cluster medium (ICM,  $i = 1$ ), which is hot ionized X-ray emitting gas. The most massive component is non-radiative dark matter ( $i = 2$ ). The particles in the two components are classical, and their velocity distributions are isotropic. Their effective degrees of freedom,  $F_i$ , are determined by the corresponding microphysics. The internal energy density is  $\epsilon_i = F_i P_i / 2$ , where  $P_i$  is the partial pressure.

Each component has the generic equation of state,

$$P_i = \rho_i \sigma_i^2 = s_i \rho_i^{\gamma_i}, \quad (1)$$

where  $\rho_i$  the density,  $\sigma_i$  is a velocity dispersion and  $s_i$  is the pseudo-entropy. Adiabatic processes leave  $s_i$  constant; objects with uniform  $s_i$  are ‘polytropes.’ The adiabatic index is given by

$$\gamma_i = 1 + \frac{2}{F_i}. \quad (2)$$

Many physical scenarios entail a condition such as equation (1). For an ideal gas, the index is the ratio of specific heats,  $\gamma = c_p / c_v$ . For a monatomic gas or a fully ionized plasma,  $F = 3$  and  $\gamma = \frac{5}{3}$ ; for a relativistic or radiation-dominated gas,  $F = 6$  and  $\gamma = \frac{4}{3}$ . Composite particles can have higher  $F$  because of their rotations and other freedoms: e.g. for a gas of mass dipoles,  $F = 5$  and  $\gamma = \frac{7}{5}$ . Polyatomic gases or SIDM ‘dark molecules’ (e.g. Alves et al. 2010; Kaplan et al. 2010) might have even higher  $F$ . An isothermal gas has infinite heat capacity, corresponding to  $F \rightarrow \infty$  and  $\gamma = 1$ . The classic Plummer (1911) model requires  $F = 10$  and  $\gamma = \frac{6}{5}$ .

Some boson-condensate and scalar field dark matter models give  $F = 2$  and  $\gamma = 2$  (Arbey, Lesgourgues & Salati 2003; Böhmer & Harko 2007; Harko 2011; Chavanis & Delfini 2011) though other values are possible (Peebles 2000). These SIDM need not be seen as consisting of distinctly localized particles (collisional or otherwise). Some theories propose phase changes in the outskirts of haloes (Arbey 2006; Slepian & Goodman 2012) which we need not consider here.

Theories of thermostatics for systems with long-range interactions (e.g. Tsallis 1988) predict that equilibria of *collisionless* spheres are polytropes, probably with non-integer  $F$  (Plastino & Plastino 1993; Nunez et al. 2006; Zavala et al. 2006; Vignat, Plastino & Plastino 2011). Two collisionless dark matter species can act together as a single anisotropic dark fluid (see Harko & Lobo 2011, 2012), but this would acquire an equation of state more complicated than equation (1).

For a single adiabatic fluid with non-singular central density and constant  $s$ , the density profile is a classical polytropic sphere (Lane 1870; Emden 1907; Chandrasekhar 1939; Viala & Horedt 1974b,a). If  $-2 < F < 10$  then the density truncates at a finite outer radius ( $R$ ), whereas the outskirts of collisionless haloes blur away as  $\rho \sim r^{-3}$ . The self-truncation of a polytropic halo seems more consistent with the steeper outer profiles observed in some clusters (Nevalainen, Markevitch & Forman 1999; Broadhurst et al. 2005; Diego et al. 2005; Umetsu & Broadhurst 2008) and galaxies (e.g. Kirihara, Miki & Mori 2013). A core of nearly uniform density fills a larger part of the sphere if  $F$  is smaller. The scale radius  $R_2$  where the density slope  $d \ln \rho / d \ln r = -2$  occurs outside the core near  $0.520R$ ,  $0.101R$  and  $0.0459R$  if  $F = 3, 8$  and  $9$ , respectively. The core boundary radius  $R_1$  (slope  $-1$ ) occurs near  $0.379R$ ,  $0.0636R$  and  $0.0285R$ , respectively (see also table A1 of Saxton 2013). Including stars or another gravitating fluid alters these proportions slightly.

Our implicit assumption of locally isotropic particle velocities is justified in a variety of DM theories: if the halo has previously been well mixed by violent relaxation and shaking of the potential; if SIDM consists of collisional particles with short mean-free-path; if the SIDM is supported by dark forces, resembling the plasma effects that mediate collisionless shocks; or if  $P$  and  $\rho$  are aspects of a smooth non-classical field (and  $\sigma^2 = P/\rho$  is merely a derived quantity). Isotropy is necessarily implied in the central pressure-supported core. If the outermost matter is also isotropic, then the halo can truncate at an outer radius,  $R$ . If the outskirts are too collisionless, then they may blur into the

cosmic background. In that case, our finite models serve as an idealized setting, and attention should focus on the core where gas cooling and SIDM effects are strongest.

Many authors interpret SIDM as point-like ( $F_2 = 3$ ) self-scattering particles (which is convenient to implement in  $N$ -body simulations). Some simulations predict oversized cluster cores, prompting suggestions that scattering cross-sections are weak ( $\zeta < 1 \text{ cm}^2 \text{ g}^{-1}$ ; Yoshida et al. 2000; Dahle, Hannestad & Sommer-Larsen 2003; Arabadjis, Bautz & Garmire 2002; Katgert, Biviano & Mazure 2004; Vogelsberger, Zavala & Loeb 2012; Rocha et al. 2013). This limitation is not the only conceptually simple possibility. Alternatively, we would vary the heat capacity: the domain  $7 \lesssim F_2 < 10$  provides realistic core sizes ( $R_1 < 0.16R$ ) without restriction on  $\zeta$  (Saxton & Wu 2008; Saxton & Ferreras 2010; Saxton 2013).

## 2.2 Formulation

The gravitational potential ( $\Phi$ ) and field ( $\mathbf{g} = -\nabla\Phi$ ) are derived from the Poisson equation, for the densities present ( $\rho_i$ ),

$$\nabla^2\Phi = 4\pi G \sum_i \rho_i. \quad (3)$$

Because each fluid density will be calculated simultaneously with the potential, our formulation implicitly includes the effect of adiabatic contraction of the dark halo, which is driven by the cooling-induced baryonic inflow (Blumenthal et al. 1986).

The mass, momentum and energy conservation equations of the system are

$$\frac{\partial}{\partial t}\rho_i + \nabla \cdot \rho_i \mathbf{v}_i = 0, \quad (4)$$

$$\frac{\partial}{\partial t}\rho_i \mathbf{v}_i + \nabla \cdot \rho_i \mathbf{v}_i \mathbf{v}_i + \nabla \rho_i \sigma_i^2 = \rho_i \mathbf{g}, \quad (5)$$

$$\frac{\partial}{\partial t}\epsilon_i + \nabla \cdot (\epsilon_i + \rho_i \sigma_i^2) \mathbf{v}_i = \rho_i \mathbf{v}_i \cdot \mathbf{g} + \mathcal{L}_i. \quad (6)$$

Here  $\mathbf{v}_i$  is the flow velocity. The source function  $\mathcal{L}_i$  in the energy equation takes account of all non-gravitational heating and cooling processes. We note that conventional ‘cooling flow’ models do not generally include the kinetic terms. Our formulation treats the kinetic terms explicitly, and all mass components participate in the gravitational interaction.

We consider stationary spherical galaxy clusters. Therefore,  $\partial/\partial t \rightarrow 0$ ,  $\partial/\partial\theta = 0$  and  $\partial/\partial\phi = 0$ . In stationary solutions, the inflow or outflow of each component ( $\dot{m}_i \equiv 4\pi r^2 \rho_i v_i$ ) is spatially constant. We assume that the dark halo is in dynamical equilibrium, with  $v_2 = 0$  and  $\dot{m}_2 = 0$  everywhere. The gas however flows inwards gradually, due to radiative cooling ( $\dot{m} = \dot{m}_1 < 0$ ). This forms a single-phase inflow. For the solutions relevant to physical galaxy clusters, the inflow is subsonic everywhere ( $0 < v_1^2 < \gamma_1 \sigma_1^2$ ).

We introduce a set of new fluid variables in terms of powers of the radial coordinate for the hydrodynamic formulation:

$$\beta_{\rho_i} \equiv \rho_i r^{F_i/2} = \dot{m}_i / 4\pi \beta_{v_i} \quad (7)$$

$$\beta_{v_i} \equiv v_i r^{(4-F_i)/2} \quad (8)$$

$$\beta_{\sigma_i} \equiv \sigma_i^2 r. \quad (9)$$

Expressing the hydrodynamic variables in these power laws softens their behaviour within the Bondi-like accretion spike that is inevitable when a point gravitating mass exists at the origin (Bondi 1952). Given values for the total mass at the outer boundary of the cluster, the mass of the gas ( $i = 1$ ) or dark matter ( $i = 2$ ) within any radius  $r$  can be obtained by numerical integration of an ODE,

$$\frac{dm_i}{dl} = 4\pi r^3 \rho_i = 4\pi \beta_{\rho_i} r^{(6-F_i)/2}, \quad (10)$$

where  $l \equiv \ln r$  is a log-radial coordinate. The form of equation (10) reveals that the mass profile  $m_i(r)$  naturally has steep inner gradients if  $F_i > 6$ . In the following equations, we abbreviate the *total* enclosed mass profile of gas plus DM plus stars as

$$m(r) = m_1(r) + m_2(r) + m_\star(r), \quad (11)$$

(see §2.5 for details of  $m_\star$ ).

The Poisson and continuity equations can decouple into a set of first-order differential equations:

$$\frac{d\beta_{v_i}}{dl} = \beta_{v_i} \left\{ \frac{4 - F_i}{2} - \frac{2\gamma_i \beta_{\sigma_i} - Gm + \frac{2}{F_i} H \beta_L r^c}{\gamma_i \beta_{\sigma_i} (1 - \mathcal{M}^2)} \right\}, \quad (12)$$

$$\frac{d\beta_{\sigma_i}}{dl} = \beta_{\sigma_i} + \frac{2 [2\gamma_i \beta_{\sigma_i} \mathcal{M}^2 - Gm - (1 - \gamma_i \mathcal{M}^2) H \beta_L r^c]}{F_i \gamma_i (1 - \mathcal{M}^2)} \quad (13)$$

$$\frac{d\beta_{\rho_i}}{dl} = \beta_{\rho_i} \left\{ \frac{F_i}{2} + \frac{2\gamma_i \beta_{\sigma_i} \mathcal{M}^2 - Gm + \frac{2}{F_i} H \beta_L r^c}{\gamma_i \beta_{\sigma_i} (1 - \mathcal{M}^2)} \right\}. \quad (14)$$

$$\frac{ds_i}{dl} = -\frac{2BH\beta_{\rho_i} r^c}{F_i \beta_{v_i} \sqrt{\beta_{\sigma_i}}} s_i. \quad (15)$$

The inflow Mach number is given by

$$\mathcal{M}_i^2 = \frac{\beta_{v_i}^2 r^{F_i-3}}{\gamma_i \beta_{\sigma_i}}, \quad (16)$$

and its profile is

$$\frac{d\mathcal{M}_i^2}{dl} = \frac{\mathcal{M}_i^2}{1 - \mathcal{M}_i^2} \left[ -4 \left( \frac{\mathcal{M}_i^2 + F_i}{F_i} \right) + \frac{2(F_i + 1)Gm}{(F_i + 2)\beta_{\sigma_i}} - (1 + \gamma_i \mathcal{M}_i^2) \frac{2H\beta_L r^c}{(F_i + 2)\beta_{\sigma_i}} \right]. \quad (17)$$

Mathematically, there is some redundancy among these ODEs. Practically, it is advantageous to integrate all of them simultaneously, because the numerical step-size control is inhibited and becomes more cautious at certain difficult parts of the radial profile, which prevents overstepping into unphysical conditions (e.g. where  $\mathcal{M}_i > 1$ ,  $\mathcal{M}_i < 0$  or  $s_i < 0$ ).

## 2.3 Gas inflow, cooling and heating

The terms  $\beta_L$ ,  $c$  and  $H$  in equations (12)–(17) describe the cooling and heating processes. The ICM in massive clusters is highly ionized, implying that  $F_1 = 3$ . The hot gas is cooled primarily by emitting thermal free–free X-rays. The thermal free–free cooling rate is  $\propto \rho_1^2 \sigma_1$  (see Rybicki & Lightman 1979), with  $\sigma_1 = \sqrt{kT/\mu m_u}$  being the thermal velocity dispersion of gas. We introduce a source term for the central AGN, which provides radiative and/or mechanical heating. We parametrize the AGN heating term as a power law of



the radial distance  $r$ . The combined heating/cooling function then takes the form:

$$\mathcal{L}_1 = A r^{-\nu} - B \rho_1^2 \sigma_1. \quad (18)$$

The parameter  $B$  is a constant depending weakly on the plasma composition (see Rybicki & Lightman 1979; Saxton & Wu 2008). The parameter  $A$  specifies the heating rate, and the index  $\nu$  determines how heating is distributed spatially. Idealized radiative heating may be represented by  $\nu = 2$ ; and centrally absorbed radiative heating by  $\nu = 2.5$ . Heating via an efficient dispersive mechanical outflow would give  $\nu \approx 0$  (i.e. uniform heating). An intermediate value would mimic the shock heating and/or mixing of ascending radio lobes from the central AGN (e.g. Brüggén & Kaiser 2001; Churazov et al. 2001; Saxton, Sutherland & Bicknell 2001; Fujita & Suzuki 2005). Hybrid mechanical and radiative heating is parametrized by  $0 < \nu < 2$ , and we take  $\nu = 1$  without losing generality. We will consider models with  $\nu = 0, 1, 2$  and  $2.5$  to investigate the effects of energy distribution by various types of AGN heating. The expression for the heating/cooling function in equation (18) implies that

$$c = \frac{7}{2} - F_1, \quad (19)$$

$$\beta_L = \frac{B \beta_{\rho_1} \sqrt{\beta_{\sigma_1}}}{\beta_{v_1}}, \quad (20)$$

and the dimensionless heating ratio

$$H \equiv \frac{B \rho_1^2 \sigma_1 - A r^{-\nu}}{B \rho_1^2 \sigma_1} = 1 - \frac{A r^{(2F_1 - 2\nu + 1)/2}}{B s_1^{1/2} \beta_{\rho_1}^{(2F_1 + 1)/F_1}}. \quad (21)$$

## 2.4 Dark matter halo

The dark matter is non-radiative; we set its cooling and heating functions to vanish ( $A = B = H = \beta_L = c = 0$ ). We assume that dark matter distribution is essentially adiabatic. The quasi-entropy,  $s_2$ , is uniform throughout the DM. This may occur if the DM was well mixed in the cluster's prehistory, and  $s_2$  measures the cumulative battering due to mergers. Alternatively,  $s_2$  might be a universal constant of the fundamental particle or dark field (e.g. Peebles 2000). Under the hydrostatic condition, the halo has  $v_2 = 0$ ,  $\mathcal{M}_2 = 0$  and  $\beta_{v_2} = 0$ . Then, we can simplify the hydrodynamic equations for  $i = 2$ , leaving equation (10) and one other gradient equation

$$\frac{d\beta_{\sigma_2}}{dl} = \beta_{\sigma_2} - \frac{2Gm}{F_2 + 2}. \quad (22)$$

A version of the equation of state (1) completes the description of halo structure:

$$\beta_{\rho_2} = (\beta_{\sigma_2}/s_2)^{F_2/2}. \quad (23)$$

Additional ODEs can be written for  $\beta_{\rho_2}$  and related quantities. These are mathematically redundant, but harmless to numerical integration routines. In this paper, we let  $F_2$  be a parameter (in the domain  $2 \leq F_2 < 10$ ). We shall investigate how the cluster properties depend on its value, and hence set some constraints on the DM microphysics.

## 2.5 cD galaxy

We insert a central galaxy in some of the clusters. The cD galaxy has a Sérsic (1968) light profile in the approximate deprojection by Prugniel & Simien (1997) (cf. the gasless galaxy model in Saxton & Ferreras 2010; Saxton 2013). The stellar density profile is given by

$$\rho_{\star}(r) = \rho_e \left( \frac{r}{R_e} \right)^{-p} e^{-b[(r/R_e)^{1/n} - 1]}, \quad (24)$$

where  $\rho_e$  is the stellar density at the half-light radius  $R_e$ . The indices  $b$  and  $p$  in the stellar density profile depend on the shape index  $n$  of the galaxy (see also Ciotti & Bertin 1999; Lima Neto, Gerbal & Márquez 1999; Márquez et al. 2000).

The stellar mass enclosed within a radius  $r$  is

$$m_{\star}(r) = 4\pi n b^{n(p-3)} e^b \rho_e R_e^3 \Gamma \left[ n(3-p), b(r/R_e)^{1/n} \right], \quad (25)$$

where  $\Gamma(a, z)$  is the lower incomplete gamma function. In the present modelling, we adopt a total stellar mass  $M_{\star} \equiv m_{\star}(\infty) = 1.8 \times 10^{11} m_{\odot}$  and effective radius  $R_e = 7.4$  kpc as fiducial values for the cD galaxy. (In the natural units of §2.6, we set  $R_e = 0.03 U_x$  and  $M_{\star} = 0.02 U_m$ .) The shape index is  $n = 4$ , corresponding to the empirical de Vaucouleurs profile (de Vaucouleurs 1948, 1953). The stellar mass profile is held fixed in the present calculations. The dark matter and intracluster gas profiles are solved consistently in the presence of stellar mass profiles of the cD galaxy.

## 2.6 Scaling and numerical integration

The dimensional constants in this system of equations are the gravitational constant  $G$  and the coefficient in the thermal free-free cooling function  $B$ . Although  $B$  depends slightly on the assumed metallicity, we may roughly set a natural unit of length:  $U_x \equiv B/G \approx 0.246$  Mpc. The velocity dispersion unit  $U_{\sigma} \equiv 1$  is chosen corresponding to the isothermal velocity dispersion of a gas at temperature  $kT = 1$  keV. The implied unit of cluster-scaled luminosity (or power) is then  $U_L \approx 1.44 \times 10^{45}$  erg s $^{-1}$ ; the mass unit is  $U_m \approx 8.91 \times 10^{12} m_{\odot}$ ; and the density unit is  $U_{\rho} \approx 6.01 \times 10^{14} m_{\odot} \text{Mpc}^{-3}$ . Some cluster models are rescalable into homologically equivalent models as long as variables such as mass, temperature and velocity dispersion are held in fixed ratios (appendices A and B, Saxton & Wu 2008). The spatial measurements and the Mach numbers are unchanged under this rescaling scheme. The composite quantities  $\dot{m}^{3/2}/m(R)$  and  $T_R/m(R)$  are also invariants. For numerical convenience, we set the units  $B = G = 1$  in our calculations.

The hydrodynamic equations for the dark matter and intracluster gas are integrated radially inwards towards the origin (the cluster centre). The minimum sufficient set of equations consists of equations (10)–(17) for the gas, (10) and (22) for the halo, along with the algebraic expressions (23), (25) and (19)–(21). By default, in ordinary regions we express the ODEs of variables  $y$  in terms of the log-radial derivatives ( $dy/dl$ ). In regions with steeper spatial gradients, the code switches to an equivalent set of ODEs in another independent variable that provides shallower derivatives locally. Near the halo's outer surface we use ODEs of the form  $dy/d\beta_{\sigma_2}$ . Wherever the inflow approaches sound speed, we use  $dy/d\mathcal{M}^2$ . In any circumstance, we employ

the embedded eighth-order Runge–Kutta Prince–Dormand method with ninth-order error estimate (Prince & Dormand 1981; Hairer, Nørsett & Wanner 2008) for the differential equation solver,<sup>1</sup> as standard lower order Runge–Kutta and Bulirsch–Stoer methods are problematic due to the stiffness of the hydrodynamic equations (at some locations). The speed and accuracy of this method enables us to survey parameter domains comprehensively, to search for extrema in the output quantities, rather than picking on arbitrary example profiles.

## 2.7 Boundary conditions and system parameters

We consider the following outer boundary conditions: (i) the outer radius of the dark halo,  $R$ ; (ii) the total mass of the cluster, which includes the dark matter, the intracluster gas and cD galaxy,  $m(R)$ ; (iii) the gas inflow rate,  $\dot{m}$ ; and (iv) the outer gas temperature,  $T_R$ , which gives the corresponding gas Mach number,  $\mathcal{M}_R$ . We impose that  $0 \leq |\mathcal{M}_R| \leq 1$  and consider a spatially uniform DM quasi-entropy  $s_2$ .

We set the fiducial total cluster mass  $m(R) = 40U_m \approx 3.57 \times 10^{14} m_\odot$ . If our models were hydrostatic, we might approximately assume  $\sigma_2 \propto \sigma_1$  in the fringes and infer the other gas variables (Frederiksen et al. 2009). This is precluded since the inflow ( $\dot{m} \neq 0$ ) requires  $\rho_1 > 0$  and  $\sigma_1 > 0$  at  $r = R$  (where the DM truncates,  $\sigma_2 = 0$ ). We pick outer boundary conditions on the gas from a cosmologically plausible domain. We set an outer gas temperature of  $kT_R = 1$  keV, representing likely conditions of shock-heated gas accreting from the cosmic background. This is a reasonable extrapolation of observed X-ray emission and Sunyaev–Zel’dovich effects, which show ICM temperatures declining to  $\sim 2$  keV around  $r \sim 2$  Mpc (e.g. Simionescu et al. 2011; Urban et al. 2011; Eckert et al. 2013; Bonamente et al. 2013; Ichikawa et al. 2013).

The gas inflow rate is  $\dot{m} = 10 m_\odot \text{ yr}^{-1}$ , which must be continuous from the outskirts inwards to the cool core and on to the central accretor. This rate is modest compared to the ‘cooling flows’ inferred for massive clusters, but great enough to overwhelm the  $\sim 0.1 m_\odot \text{ yr}^{-1}$  effects of a cD galaxy’s stellar winds and supernovae (e.g. White & Chevalier 1984; Loewenstein & Mathews 1987; Sarazin & White 1987; Vedder, Trester & Canizares 1988; Sarazin & Ashe 1989; Mathews & Brighenti 2003). We seek solutions in which the baryon fraction within  $< R$  matches a predefined cosmic value, including the cosmic mean ( $\approx 0.16$ ). Fortunately, these realistic models obtain outer gas densities ( $\rho_1$ ) comparable to the cosmic mean. The subtle effects of varying  $T_R$  and  $\dot{m}$  were shown in Saxton & Wu (2008).

By integrating radially inwards from physically justified external and global properties, we avoid the sensitivity to boundary conditions suffered by some other cooling flow models (e.g. in isolated elliptical galaxies; Vedder, Trester & Canizares 1988). Integrating out from (unlucky) ad hoc central conditions can lead to unphysically high temperatures in the outskirts. In a realistic universe, however, the cosmic background gas is indifferent to

the properties of a cluster until it accretes. It is the global mass and size of a cluster that constrain its internal details, not the details that control the bulk. It might be interesting to explore these sensitivities, but in this work we implement the most robust method: computing from the outside inwards.

Once the integrator arrives at the origin, we test the consistency of conditions there. The integration from  $r = R$  to the origin determines the mass profiles of the DM and the intracluster gas and hence the central values  $m_1(0)$  and  $m_2(0)$ . We may define

$$m_* \equiv m(0) = m_1(0) + m_2(0) + m_\star(0), \quad (26)$$

which is essentially the residual mass at the cluster centre. The Prugniel & Simien (1997) stellar profile does not contribute any mass at the origin, i.e.  $m_\star(0) = 0$ . The residual mass  $m_*$  implies a point-like mass concentration at the origin, and we may interpret it as a massive black hole at the centre of the cluster. We stress that  $m_*$  is not an input parameter; it is a non-trivial output of each model calculation. After integration, both the inner and outer boundary conditions are known, and we retrospectively find the total gas and DM masses:  $M_1 = m_1(R) - m_1(0)$  and  $M_2 = m_2(R) - m_2(0)$ . The baryon fraction follows directly.

## 2.8 Allowed regions for physical solutions in the parameter space

In the absence of the cD galaxy, the integration of the hydrodynamic equations of the clusters gives four types of solutions, corresponding to four distinct regions in the parameter space. In Saxton & Wu (2008), they were identified as follows.

- (i) the ‘*too cold*’ zone: overcooling occurs at some finite radius. A zero-temperature shell falls freely inwards. This is inconsistent with the stationary assumption in the model.
- (ii) the ‘*too fast*’ zone: a supersonic break occurs at some radius. This forbids a two-way communication between the interior and exterior, giving inconsistent mass fluxes.
- (iii) the ‘*levity*’ zone: the pressure support in the cluster is insufficient, leading to an unphysical negative central mass.
- (iv) the ‘*deep*’ zone: the balance between radiative cooling of the gas and accretion warming everywhere ensures that cold and fast inflow catastrophes do not occur in the cluster.

Solutions corresponding to (i), (ii) and (iii) are unphysical. Stationary solutions corresponding to (iv) subject to the boundary conditions are acceptable physical solutions. In the presence of a cD galaxy, the four types of solutions and their corresponding distinguishable zones in the parameters are also identified. However, the zone borders for the cases with and without a central cD galaxy differ in detail.

## 3 RESULTS

### 3.1 Global properties and central mass

Unsteady overcooling could cause a discontinuity to form at a certain radius. This can be avoided, when a sufficiently massive central object is present as an accretor, since heating due to the accretion process counteracts radiative cooling.

<sup>1</sup> We use mathematical routines from the GNU SCIENTIFIC LIBRARY (<http://www.gnu.org/software/gsl/>).

For the parameters that we have considered, all steady solutions have positive central mass,  $m_* > 0$ . The main parameters to be explored are  $(F_2, R, s_2, \mathcal{M}_R)$ . By comprehensive numerical searches over  $(s_2, \mathcal{M}_R)$ , we map the landscape of the minimal  $m_*$  across the parameter space. Optimization routines can iterate to the best solution (within round-off) after integrating the model profiles at a few hundred  $\mathcal{M}_R$  trial values, and a few hundred  $s_2$  values for each of those. Painstaking reiteration of this process at different  $(F_2, R)$  yields maps such as Fig. 1, where black contours show the minimal  $m_*$  and red shows cluster baryon fractions.

We previously explored the effects of  $m(R)$ ,  $T_R$ ,  $\dot{m}$  and  $F_2$  upon the halo radius  $R$  (for given baryon fraction) and for the possible values of the central point-like mass in the clusters without a cD galaxy (Saxton & Wu 2008). Assuming a standard mass  $m(R)$ , these are the main findings.

- (i) When the baryon fraction is fixed, larger  $F_2$  gives smaller  $m_*$ , i.e. a larger value for the internal degree of freedom of the dark matter particles gives a small mass for the central point-like object.
- (ii) Large gas inflow rate  $\dot{m}$  implies a larger limit for the central point-mass  $m_*$ , and greater sensitivity of  $m_*$  to  $F_2$ .
- (iii) For a given baryon mass fraction, the cluster halo radius  $R$  decreases when  $\dot{m}$  increases.
- (iv) Raising the outer gas temperature  $T_R$  reduces  $R$ , but leaves the  $m_*$  map unchanged.

Observations have shown that central black holes in many galaxies have masses  $\sim 10^6\text{--}10^9 m_\odot$  (see e.g. Gültekin et al. 2009; Graham et al. 2011). Our cluster models provide minimal  $m_*$  in this range if the degrees of freedom of dark matter may be in the range  $7 \lesssim F_2 < 10$ . For smaller  $F_2$ , the predicted  $m_*$  are excessively massive. (Note that values of  $F_2 > 10$  cannot form a finite mass within a finite radius in our cluster model.) This range of  $F_2$  is consistent with polytropic halo fits to the scaling relations of disc galaxies, which imply  $F_2 \approx 9.6$  (Nunez et al. 2006; Zavala et al. 2006). Fitting the kinematics of planetary nebulae and stellar tracers in elliptical galaxies prefers a range  $7 \lesssim F_2 \lesssim 9$  (Saxton & Ferreras 2010). For our choices of  $\sim 1$  keV gas temperatures at the cluster outskirts, empirically plausible cluster halo radii of a few Mpc imply that gas inflows are more modest ( $< 100 m_\odot \text{ yr}^{-1}$ ) than some X-ray observations implied.

Here, we consider a more general situation: the cluster contains a cD galaxy which provides a significant additional gravitational field in central regions, and the AGN within the cD galaxy provides radiative and/or mechanical heating to the intracluster gas. The central mass limits arise due to local thresholds of overcooling and supersonic catastrophes in the inner regions. This is affected by the central contraction of the halo by gas inflow (which depends on  $F_2$ ). However, since the stellar mass of a cD elliptical galaxy is dynamically significant at kiloparsec radii, it is desirable to test how it influences the domain of steady solutions.

We find that the inclusion of the cD galaxy (lower panel, Fig.1) leaves the cosmic composition tracks unchanged (red dotted contours). This is somewhat unsurprising: in a more global view, the mass contribution of the cD galaxy is an insignificant detail compared to the overall mass distribution of the cluster. The global properties of the cluster (e.g. mass, temperature and radius relations) are essentially unaffected

by the localized perturbation in the innermost region of the cluster core.

However the presence of the cD galaxy has a subtle but notable effect on the central mass limit,  $m_*$ . Without the galaxy (upper panel, black contours of Fig. 1) there is a large domain where the clusters with cosmic compositions always have a central object  $m_* > 10^{10} m_\odot$  if  $F_2 \lesssim 7$ . We infer  $F_2 \gtrsim 7$  on astronomical grounds. When the galaxy is included, the  $m_*$  limits drop by at most a factor  $\sim 3$  for cases where the halo has  $F_2 < 7$  (see the lower panel in Fig. 1). The mass limits for haloes with  $F_2 \gtrsim 7$  are not significantly affected (the tight black contours on the right-hand side of each panel). Thus, the presence of a galaxy's stellar mass slightly lessens the observational exclusion of low  $F_2$ . In the context of the SIDM model, the requirement of realistic central black holes still favours a larger number of thermal degrees of freedom ( $F_2 \gtrsim 7$ ).

We may interpret this finding as follows. In effect, the stellar component is analogous to an extra halo component with shallow gradients. It does not fundamentally change the local vulnerability of the gas flow to breakage in supersonic rips nor cooling catastrophes. Nor does the galaxy affect the compressibility and dynamical characteristics of the DM. The preference for high  $F_2$  is a consequence of the dark matter's weak pressure response to density variations. Steep central density gradients are required to provide pressure support in the interior, and those high densities enable a massive dark spike around a smaller point-mass.

The inclusion of an AGN-like heating function ( $A > 0$ ) has a moderate effect on the size relations among clusters. Figure 2 shows the results of different heating rates upon minimal  $m_*$  clusters of given radius ( $R$ ), for fixed inflow rate ( $\dot{m} = 10 m_\odot \text{ yr}^{-1}$ ), gas surface temperature ( $T_R = 1 \text{ keV}$ ), total mass and halo physics ( $F_2 = 8$ ). If the heating is of the order of the fiducial power ( $U_L \approx 1.44 \times 10^{45} \text{ erg s}^{-1}$ ), then we find no stationary solutions for clusters with this choice of  $(\dot{m}, m, T_R, F_2)$ . At a given baryon fraction, heating at rates of  $10^{-2} U_L$  results in a smaller cluster radius ( $R$ ) than in unheated clusters (upper curves of Fig. 2). If the heating is reduced to  $\lesssim 10^{-4} U_L$ , then the size and composition relations are indistinguishable from unheated models (lower curves of Fig. 2). Comparing the panels of Fig. 2 shows that the global rate of heating is the most decisive parameter; the radial index of the heating function makes little difference in the domain we explored ( $\nu = 0, 1, 2$  and  $2.5$ ). For larger  $\nu$  (more concentrated heating), the AGN is less effective at reducing cooling at cluster core scales, and the results become marginally less sensitive to the power parameter  $A$ . Qualitatively, non-gravitational heating enables denser gas profiles to avoid local overcooling catastrophes; the 'too cold' zone occupies less of the configuration-space. At a fixed cluster size  $R$ , greater gas fractions are possible. At a fixed gas fraction, clusters can be more compact. Heating is more effective if it occurs in the kpc-scale cool core, less effective if it concentrates in the hot inner nucleus.

Whether or not heating affects the cluster size relations is independent of the halo microphysics. We confirmed this by calculating  $F_2 = 3$  results equivalent to the  $F_2 = 8$  models illustrated in Fig. 2. However, the heat sensitivity of the minimal central mass ( $m_*$ ) does depend on the dark matter degrees of freedom. Fig. 3 shows how strong heating can lower the limiting  $m_*$  by up to a few tens of percent

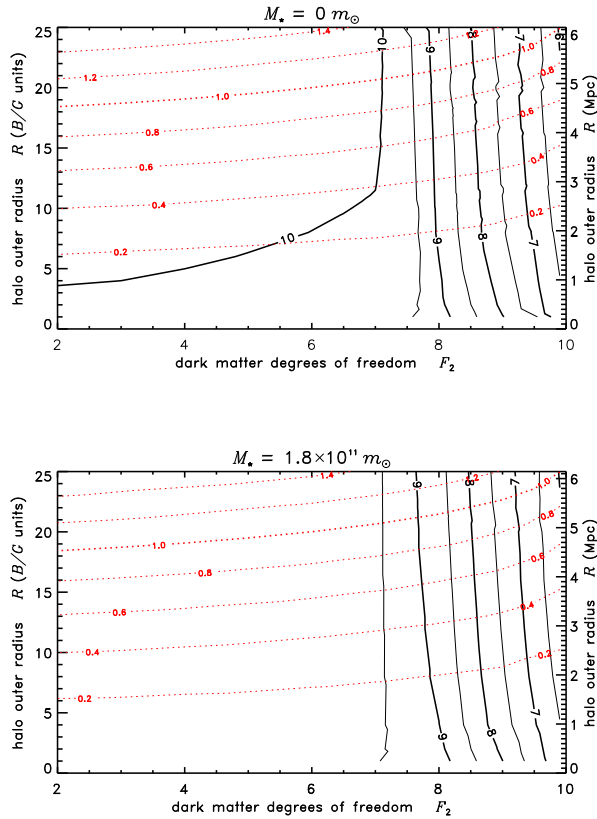


**Figure 1.** Relations between cluster radius  $R$ , the dark matter degrees of freedom  $F_2$  and the minimum central mass (the mass for the central SMBH). Black (solid) contours show logarithms of the minimal central mass, in solar units ( $\log_{10}(m_*/m_\odot)$ ), found by minimizing over  $(s_2, \mathcal{M}_R)$ . Red (dotted) curves are tracks where the baryon mass fraction is a certain multiple of a ‘cosmic’ reference value (0.16). The top panel shows the clusters without a central cD galaxy (i.e.  $M_\star = 0$ ). The bottom panel shows the cluster containing a cD galaxy with  $M_\star = 1.8 \times 10^{11} m_\odot$ .

when  $F_2 = 8$ . When there are fewer degrees of freedom (e.g.  $F_2 = 3$  calculations) the  $m_*$  versus  $R$  curves differ negligibly between  $10^{-2}U_L$ ,  $10^{-3}U_L$ ,  $10^{-4}U_L$  and unheated clusters. The same is found when the polytropic halo is replaced by the popular but cuspy ‘NFW’ profile of collisionless DM simulations (Navarro, Frenk & White 1996). Appendix A illustrates and summarizes the results of these variants. The central mass and global scaling properties of NFW clusters resemble those of  $F_2 \approx 3$  clusters: the minimal  $m_*$  is ultra-massive, and AGN heating has negligible effect compared to the introduction of the cD galaxy potential.

### 3.2 Density profiles

We generally obtain a power-law-like gas density profile with the power-law index  $\approx 1$  (top row, Figs 4 and 5). This is similar to the profiles in the conventional ‘cooling flow’ models (see e.g. Cowie & Binney 1977; Fabian & Nulsen 1977). There is usually a subtle break in the slope at a kpc radius or smaller. The innermost gas profile below a few pc is  $\rho_1 \sim r^{-1.5}$ , like a Bondi (1952) accretion spike.

The DM has a more complicated density profile. A parsec-scale dark density spike surrounds the

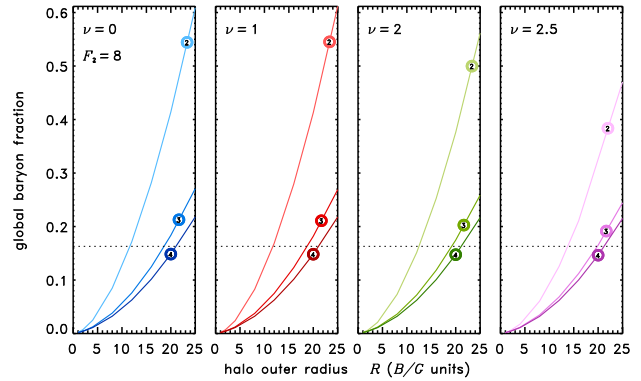


**Figure 2.** Baryon mass fraction as a function of halo radius ( $R$ ) for clusters with a cD galaxy and spatially distributed heating by the AGN ( $Ar^{-\nu}$ ). The cluster parameters are  $F_2 = 8$ ,  $T_R = 1\text{keV}$ ,  $\dot{m} = 10m_\odot \text{yr}^{-1}$ . Curves indicate the heating power as labelled:  $10^{-2}U_L$ ,  $10^{-3}U_L$ ,  $10^{-4}U_L$  (where the fiducial luminosity  $U_L \approx 1.44 \times 10^{45} \text{erg s}^{-1}$ ). Panels from left to right show: spatially uniform heating ( $\nu = 0$ ); the a somewhat concentrated heater ( $\nu = 1$ ); the radiation-like heating ( $\nu = 2$ ); and a more concentrated model ( $\nu = 2.5$ ). The dotted lines indicate a ‘cosmic’ baryon fraction.

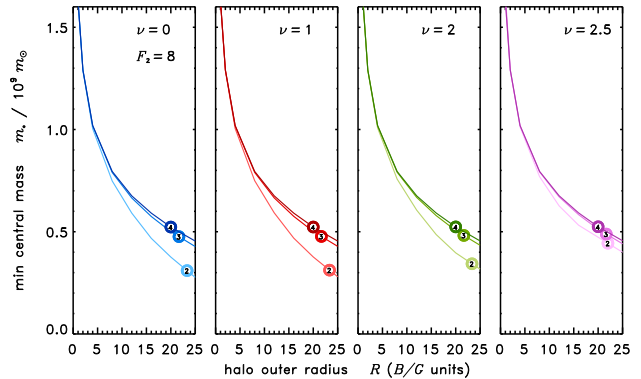


**Figure 3.** Minimal central point-mass ( $m_*$ ) as a function of halo radius ( $R$ ) for clusters with a cD galaxy and spatially distributed heating. The cluster parameters and heating power of the AGN correspond to the panels and curves in Fig. 2.

central mass. This is not accreting material like the gas cusp, but an adiabatic structure supported by its own pressure. This inner subsystem is a gravitational domain-of-influence belonging to the central mass and the spike material itself (similar to e.g. Huntley & Saslaw 1975; Quinlan, Hernquist & Sigurdsson 1995; Gondolo & Silk 1999; Ullio, Zhao & Kamionkowski 2001; MacMillan & Henriksen 2002). Even if dark matter were collisionless in extragalactic conditions, it becomes effectively collisional in the nuclear region, via scattering with stars there (Ilyin, Zybin & Gurevich 2004; Gnedin & Primack 2004; Merritt 2004; Zelnikov & Vasiliev 2005; Vasiliev & Zelnikov 2008; Merritt 2010). In the Newtonian (weak gravity) regions of the spike, the dark density profile depends on the number of effective thermal degrees of freedom,  $\rho_2 \sim r^{-F_2/2}$ . Now we find that adding the stellar mass profile of a cD galaxy has no significant effect on the occurrence of spikes, nor the spike’s density gradient. However, for the minimal  $m_*$  solutions, the cD galaxy envi-



ronment makes the spike an order of magnitude less dense (and lower velocity dispersion by a smaller factor).

Outside the spike, the density is almost uniform throughout a core spanning 10 kpc to several 100 kpc for plausible cluster models. Outside this core, the dark density fringe declines smoothly towards zero at the truncation radius  $R$ . We might define the edge of the dark core as the radius where the density index passes specific values (e.g.  $d \ln \rho / d \ln r = -2$  at  $r = R_2$ , or slope  $-1$  at  $r = R_1$ ). These locations are marked with arrows in Figs 4 and 5. Similarly to single-fluid polytropes, the size of the cluster's dark matter core depends on  $R$  and the dark matter degrees of freedom,  $F_2$ . In the minimal  $m_*$  solutions shown in Figs 4 and 5, the core is clearly smaller when  $F_2 = 9$  than when  $F_2 = 3$ . For greater degrees of freedom, the core is generally smaller. The inclusion of a kpc-sized central galaxy only shrinks the dark core by  $\lesssim 1\%$ . For our standard clusters with cD galaxy and cosmic composition, when  $F_2 = 8, 9, 9.5$  and  $9.9$  the core sizes give  $R_1 \approx 366, 187, 98.5, 21.7$  kpc, respectively. In hindsight, our standard models seem a bit diffuse and colder than observed clusters. This is easily remedied: the radii would shrink if  $|\dot{m}|$  or  $T_R$  were increased at the outer boundary. Alternatively, under the scaling homologies, the model is equivalent to a cluster a few times hotter and more massive than standard  $4 \times 10^{14} m_\odot$  (whilst keeping the same radial dimensions).

### 3.3 Temperature profiles

If self-gravity and the kinetic terms in the hydrodynamics are ignored (in the conventional ‘cooling flow’ models), gas temperatures in the inner core region of a cluster can reach zero when runaway radiative cooling develops. As a result, the ratio of peak to coolest gas temperatures  $T_{\max}/T_{\min}$  is expected to be very large throughout the core, which is inconsistent with the observations that  $T_{\max}/T_{\min} \sim (2-5)$  for most cool-core clusters (Kaastra et al. 2001; Tamura et al. 2001; Peterson et al. 2001; Böhringer et al. 2001; Sakelliou et al. 2002; Etori et al. 2002; Peterson et al. 2003; Voigt & Fabian 2004; Bauer et al. 2005; Zhang et al. 2006; Werner et al. 2006; Fujita et al. 2008; Takahashi et al. 2009; Bulbul et al. 2012). We demonstrate that when self-gravity and kinetic terms are included in the hydrodynamics, the gas is a cooling-induced inflow and the ICM floor temperature ( $T_{\min}$ ) is non-zero. This is due to the fact that the radiative cooling of the intracluster gas is counterbalanced by accretion warming, averting the runaway cooling process. The accretion effect tends to be larger for larger  $m_*$  or when a cD galaxy is present. Although runaway cooling can occur (in the ‘too cold’ configurations), in more realistic settings  $T_{\min}$  is non-zero, and the finite value of the ( $T_{\max}/T_{\min}$ ) ratio depends on the gas inflow parameters and other global parameters of the clusters (Saxton & Wu 2008).

The lower panels of Figs 4 and 5 depict temperature profiles of some minimal  $m_*$  clusters with and without the cD galaxy, for  $F_2 = 3$  and  $F_2 = 9$  haloes, in cases matching the standard cosmic baryon fraction. Gas temperature profiles are generally S-shaped curves: hottest around the central accretor; a minimum ( $T_{\min}$  at  $R_{\min}$ ) farther out in the ‘cool core’; a peak ( $T_{\max}$ ) at  $R_{\max} \sim \text{Mpc}$  radii; then a decline in the outer fringe. The coldest layer of the cool core occurs at radii  $R_{\min}$  of a few kpc to tens of kpc. The minimal  $m_*$

model always provides the most extreme ICM temperature decrement (greatest  $T_{\max}/T_{\min}$ ), other solutions show less temperature variation. All else being equal,  $R_{\max}$  is smaller if  $F_2$  is larger. Otherwise this peak location is mainly dependent on the cluster radius  $R$ , but somewhat affected by outer boundary properties ( $\dot{m}, \mathcal{M}_R, T_R$ ). The floor  $T_{\min}$  is controlled by accretion and heating in central regions. Adjusting these quantities can provide fits to observed X-ray temperature profiles, comparable to the NFW-based parametric fits of Vikhlinin et al. (2006) (but without needing to omit data in the inner tens of kpc). See Appendix B for examples. Each physically self-consistent fit entails exploration of a large parameter-space, which is best left for a dedicated paper.

Fig. 6 shows the relation between  $T_{\max}/T_{\min}$  and  $m_*$  for various types of clusters with different AGN and cD conditions (but all with  $F_2 = 8$  and  $R = 16U_x \approx 4$  Mpc identically). When there is no cD galaxy in these clusters the ( $T_{\max}/T_{\min}$ ) ratios are  $\sim 1 - 40$  (black dashed curve in Fig. 6). The relation between ( $T_{\max}/T_{\min}$ ) and  $m_*$  is not easily described in terms of a simple function. It is non-monotonic if  $F_2 > 6$ . However, we can see that the ( $T_{\max}/T_{\min}$ ) ratio can be reduced when  $m_*$  is sufficiently large. Thus, in principle ( $T_{\max}/T_{\min}$ )  $\approx 1$  can be attained for very large  $m_*$ . In such situations, there is no temperature minimum; the ICM becomes continually hotter nearer the centre (like a non-cool-core cluster).

When a cD galaxy is present in the cluster, its stellar mass strengthens the power generation via accretion, counteracting the radiative cooling of the gas in the cluster core region. This raises  $T_{\min}$  substantially at  $r \lesssim 30$  kpc and hence reduces the ( $T_{\max}/T_{\min}$ ) ratio (grey curve in Fig. 6). The stellar mass profile of the cD galaxy distributes the accretion power smoothly over regions at kpc radii, rather than concentrated in compact region around the central point-mass. The temperature floor is raised accordingly, creating a softer temperature gradient in the intracluster gas around  $\sim 10^1$  kpc radii. Note that the presence of the cD galaxy may boost  $T_{\min}$  by some factors (about three for minimal  $m_*$  cases), but  $T_{\max}$  does not change significantly.

Next, we consider the addition of heating by an AGN in the cD galaxy. We assume that the AGN heating is steady, as the duty cycles of AGN may be on time-scales of million years and the global dynamical time-scales of the cluster are about hundred million years. We parametrized the distribution of AGN power in the intracluster gas by means of spatial power laws with various indices,  $\nu = 0, 1, 2$  and  $2.5$ . Our calculations have shown that for  $F_2 = 8$  clusters in the presence of a cD galaxy, the attainable ranges of  $T_{\max}/T_{\min}$  are very similar for different types of AGN distributed heating (the colour curves in Fig. 6). Moreover, they are also very similar to the case with an inactive AGN (i.e. just a cD galaxy). For  $F_2 = 8$  clusters, the curves of different  $\nu$  are similar but displaced in  $m_*$ . For  $F_2 = 3$  or clusters with the ‘NFW’ halo profile, the AGN heating increases the  $T_{\max}/T_{\min}$  ratio at any given  $m_*$  (Appendix A). Interestingly, the AGN-heated  $T_{\max}/T_{\min}-m_*$  curves approach the curve for an inactive galaxy when the value of  $\nu$  increases. Nevertheless, the heating distribution index  $\nu$  influences the minimum value of  $m_*$  possible in the model. This is not too surprising as centrally concentrated AGN heating and accretional heating via the presence of cD galaxy share a

similarity: the heat generation in both cases is in the core region of the cluster.

In summary, the temperature floor  $T_{\min}$  can be raised essentially by the presence of some heating sources to counterbalance the radiative losses of the gas. The heating sources can be hydrodynamical heating (via accretion on to a point-mass or cD galaxy) and/or power from an AGN. Accretion heating via the presence of a cD galaxy is able to produce  $T_{\max}/T_{\min}$  compatible with presently available observations. The distributed heating of an AGN may lower the  $T_{\max}/T_{\min}$  ratio but appears less influential than the cD galaxy's gravity. Nevertheless, the lower limit for  $m_*$  depends on how the AGN power is distributed spatially and/or on whether or not an AGN is present.

## 4 DISCUSSION

### 4.1 Symmetry and extra gas processes

This paper emphasizes the role of the cD galaxy in a cooling ICM in a naturally cored galaxy cluster. Our treatment of the gas does not contain all conceivable processes, and we should briefly consider the relevance of extra physics.

We warn that our findings might not be relevant for systems that violate the spherical, isotropic, stationary assumptions. The constraints might change in a real cluster that is distorted by non-spherical or anisotropic effects: bulk rotation, streaming motions, massive substructures, gross departures from spherical symmetry, local anisotropies and non-thermal plasma effects, or magnetically dominated pressure. Our models are also inapplicable to significantly non-stationary clusters, e.g. during violent mergers. Such convulsions would of course induce global mixing and shocks, temporarily erasing the cooling gas inflows that we intended to explain.

Among the smaller scale physics, we intentionally omit the mass sink terms (describing condensation of dense cold blobs from the ICM) that feature in other cooling flow models (especially at galaxy scales, e.g. Mathews & Brighenti 2003). Our justification is empirical: the cool condensates and star formation are not observed in the required amounts (Donahue & Voit 2004). The inflowing matter must have a different fate, deep in the nuclear regions. We also omit potential complications, such as radiation pressure, magnetic field geometry and rotation, which could determine the detailed internal anatomy of the AGN at sub parsec radii. Our goal is to explain the cluster structure without depending too much on microscopic complications.

Gas turbulence could boost the effective internal heat capacity of the ICM, due to the kinetic energy density of eddies. Observations suggest that this does not add more than a few tenths of the thermal pressure component (e.g. Sanders et al. 2010) which would imply  $3 < F_1 < 4$  (and closer to the lower limit). A slightly enlarged  $F_1$  may defer overcooling in particular models, loosening the constraint of the 'too cold' zone in configuration space (but probably not enough to make a qualitative difference to  $m_*$  limits and cluster compactness).

The fluid description depends on the mean free path (mfp) of ICM particles ( $\propto \sigma^4/\rho$ ) being much smaller than  $r$ . Processes that depend on scattering (especially the free-free

cooling function) are effectively blurred across that length-scale. Overcooling catastrophes might be averted in some marginal cases (relaxing constraints in the configuration space). Such a semiclassical model is not expressible as an initial value problem of ODEs, and would need a different numerical scheme. Fortunately, for our most realistic cluster solutions (in terms of  $m_*$  and size) the estimated mfp in the cool core and Mpc outskirts turns out to be at most a few percent of  $r$ , justifying the fluid approximation. Only in the nuclear region ( $r \lesssim 0.1$  pc) does the gas become collisionless in mfp terms. Since the overcooling catastrophes occur at kpc radii, this aspect of AGN anatomy will not affect the key conclusions of this paper.

Our present formulation omits thermal conduction. This process would introduce another energy exchange term in  $\mathcal{L}_1$ , ( $\propto \nabla \cdot (\sigma_1^5 \nabla \sigma_1^2)$ ; Sarazin 1988, section 5.4.2) and require specification of an outer boundary condition on  $\nabla \sigma_1^2$ . Qualitatively, we would expect conduction to soften temperature gradients, by spreading warmth from the inner accretion region outwards to the cooling core. Previous works emphasized conductive heating of the core by the outskirts (e.g. Narayan & Medvedev 2001; Ruszkowski & Begelman 2002; Voigt & Fabian 2004; Ruszkowski & Oh 2010). The ICM temperature floor  $T_{\min}$  might be raised further than in the present models, and the highest  $T_{\max}$  values would also decrease. Realistic temperature ranges ( $T_{\max}/T_{\min} < 5$ ) might occur for a broader domain of cluster parameters. In the inner sub parsec accretion region, conduction could dominate over emission, dimming the central X-ray source. Such effects are probably insensitive to  $F_2$  halo physics and cD galaxy profile, but may make an interesting topic for future modelling.

### 4.2 Jeans stability and dark collapse

As an indicator of local gravitational stability, we can calculate a Jeans radius at any layer of the cluster:

$$r_J \equiv \sqrt{\frac{\pi \gamma \sigma^2}{4G\rho}}. \quad (27)$$

Stability would be indicated when the Jeans radius is greater than the radius of a particular layer locally,  $r_J > r$ . In the absence of a cD galaxy, Saxton & Wu (2008) found the gas to be stable everywhere, and increasingly stable in the interior (grey lines in the left-hand panels of Fig. 7). Now we find that the addition of a cD galaxy stellar mass profile can subtly flatten the profile of  $r_J/r$  for gas, at radii comparable to  $R_e$  (see the grey curves of the right-hand panels of Fig. 7, and compare to the upper panels). By this criterion, the gas inflow remains stable in the presence of the galaxy, just as it was without a cD galaxy.

The corresponding property of the dark halo depends on the thermal degrees of freedom,  $F_2$ . For cases with  $F_2 < 6$  the central regions of the halo are increasingly stable, similarly to the gas. However for  $F_2 > 6$  the dark spike rises towards the threshold of instability ( $r_J \approx r$ ) in a deep interior within  $r < 10$  pc. This is a manifestation of the classic dynamical instability of pure polytropic spheres with high index (Ritter 1878; Emden 1907; Chandrasekhar 1939, p. 51). Simplistically, for large  $F$  the pressure response to a local perturbative compression may be insufficient to restore dy-

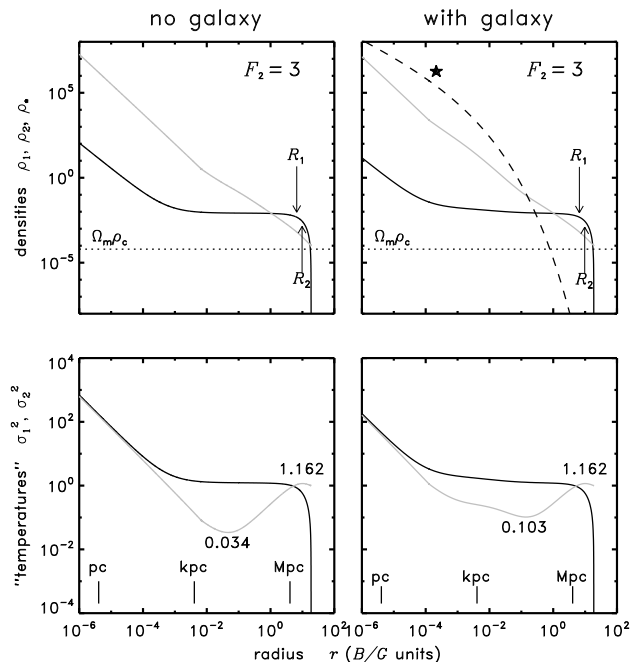


**Figure 4.** Radial profiles of density (top row), and ‘temperatures’ or velocity dispersions (bottom) for minimal  $m_*$  clusters. Gas is shown grey; dark matter in solid black curves. The dotted line is the standard cosmic mean density; the dashed curve is the stellar density. These particular solutions were chosen as those with the minimum central mass, and thus a large ICM temperature variation. This figure shows cases with  $F_2 = 3$  dark matter degrees of freedom, analogous to a particles of a monatomic plasma. In the left-hand column there is no cD galaxy (as in Saxton & Wu 2008); in the right-hand column the fiducial galaxy has been added. Arrows mark  $R_1$  and  $R_2$ , indicators of core sizes in terms of the density slope ( $d \ln \rho / d \ln r = -1, -2$  at  $R_1, R_2$ ). The gravitational effect of the cD galaxy raises the gas floor temperature by a factor  $\approx 3$ . Local extrema of the gas temperature are annotated. The three ticks in the bottom panels show the 1pc, 1kpc and 1Mpc radii.

namical equilibrium. We find that the  $r_J/r$  behaviour persists after introducing the distributed stellar mass of a cD galaxy. Comparing minimal  $m_*$  models with and without the galaxy, the radial gradients of  $r_J$  are only subtly changed. This phenomenon occurs at such small radii that the introduction of the stellar background mass distribution — mainly farther out at kiloparsec scales — makes no significant effect.

The upturn of  $r/r_J$  for the inner part of the dark halo implies that external perturbations could cause it to detach and collapse on its dynamical time-scale. Gas does not participate directly, so the implosion is dark, evading the limits of Eddington (1918) and Soltan (1982). Arrows in the lower panels of Fig. 7 indicate radii enclosing  $10^7, 10^8$  and  $10^9 m_\odot$ . For cluster-sized solutions and large  $F_2$ , the fragile part of the halo is up to a billion solar masses. This implies that an SMBH could grow substantially in a ‘dark gulp’ (Saxton & Wu 2008). This process may alleviate the need for conspicuously luminous gas accretion, and explain the rapid formation of SMBH implied by the existence of powerful quasars at high redshifts,  $z > 6.4$  (e.g. Fan et al. 2004; Mortlock et al. 2011). Dark gulping may be a fac-

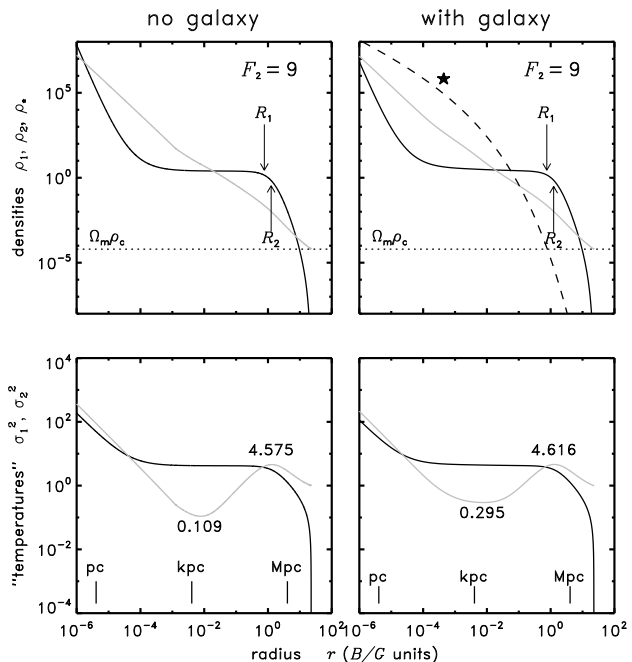


**Figure 5.** Density and velocity dispersion profiles for minimal  $m_*$  cluster models as in Fig. 4 but now with greater dark matter heat capacity,  $F_2 = 9$ . The dark matter core is smaller. Like the  $F_2 = 3$  case, the floor temperature of the gas is raised by a factor of  $\approx 3$ .

tor counteracting a more modern issue of black hole demographics: it is thought that some merged black holes can eject from the host galaxy due to gravity-wave recoil (e.g. Haiman 2004; Baker et al. 2006; Campanelli et al. 2007a,b; Schnittman & Buonanno 2007; Lousto & Zlochower 2011, 2013). Our scenario suggests that a replacement SMBH could condense naturally at the centre of the dark halo (e.g. as in NGC 1275; Shields & Bonning 2013). It is reassuring to confirm that this ‘gulping’ prediction is essentially unchanged by the cD galaxy’s stellar profile. If the such events can be prevented (in the high- $F_2$  SIDM context) it would require additional non-gravitational physics. The persistence of collisionless stars in their orbits can have a stabilizing effect on the surrounding polytropic halo (Saxton 2013). Details of the collapse modes must depend non-trivially upon the stellar and dark density profiles in the nuclear region (as in the ‘skotoseismology’ of gasless galaxies; Saxton 2013).

## 5 CONCLUSIONS

We generalize our previous work on hydrodynamical structures and stability properties of stationary, locally isotropic, spherical galaxy clusters. This basic model included self-gravity and the kinetic terms, which were missing from many conventional analyses of hydrodynamics of galaxy clusters, enabling us to correct and improve upon past understandings of cooling-induced gas inflows. Combined with observational constraints, our study gives insights into the dark matter physics. In this work, we investigate the effects of the presence of a cD galaxy and central AGN. The stellar mass profile of a cD galaxy exerts a gravitational influence in the

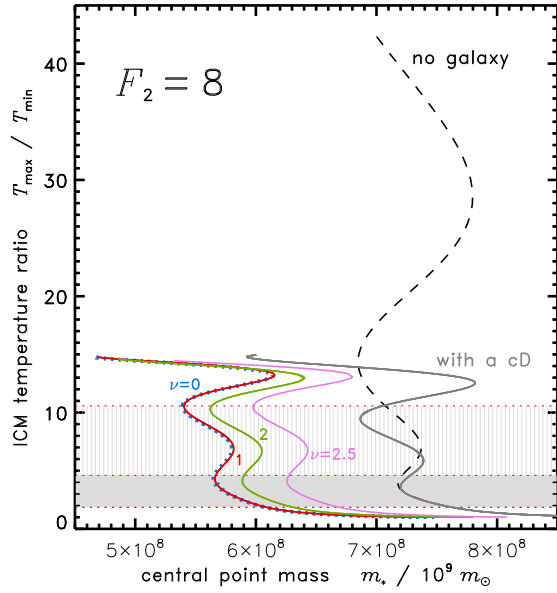


**Figure 6.** The  $(T_{\max}/T_{\min})$  ratio of the intracluster gas for cluster models with  $F_2 = 8$  and radius  $R = 16$ , along the borders of the ‘deep zone’ continuous models. The horizontal axis is the central point-mass  $m_*$ . The dashed black curve shows the ratios for clusters without a cD galaxy. The grey curve shows results with an inactive cD galaxy. Coloured curves show the ratio for the clusters with an AGN in the cD galaxy. The power of the AGN is  $10^{-2}U_L$  and the spatial indices of the AGN heating functions are  $\nu = 0, 1, 2$  and  $2.5$  respectively. The grey shaded band shows the normal range of cool-cored clusters; the lined region includes Centaurus. The gravity of the cD galaxy is able to significantly lower the  $(T_{\max}/T_{\min})$  ratio. The form of heating function affects the attainable value of central point-mass  $m_*$ .

cluster interior, and the AGN provides distributed heating into intracluster gas.

We obtain exhaustive constraints on the profile and central object of a galaxy cluster with gas inflows, within the scope of our assumptions and with the stated ingredients. Our results depend on the stationarity, spherical symmetry and isotropy of the cluster and the active central galaxy. The constraints might be eluded, to an unknowable extent, if these conditions are unmet. With that caveat, we summarize our findings as follows.

(i) The cD galaxy provides additional accretion warming (due to stellar mass distributed at kiloparsec scales). This raises the floor temperature of the intracluster gas and hence reduces the temperature gradients in the cool core of the cluster. Hence, a finite temperature floor in the intracluster gas can be attained in the presence of a cD galaxy regardless of distributed heating by an AGN or other non-gravitational heat sources.

(ii) For given intracluster gas and dark halo masses, gas inflow rate and external temperature, minimal  $m_*$  clusters with AGN distributed heating exceeding  $\gtrsim 10^{41}$  erg s $^{-1}$  are slightly more compact than equivalent unheated models.

(iii) Smaller dark matter cores (less than a few hundred kpc) still require large degrees of freedom  $F_2$  for the dark matter. On these grounds alone, the preferred range is

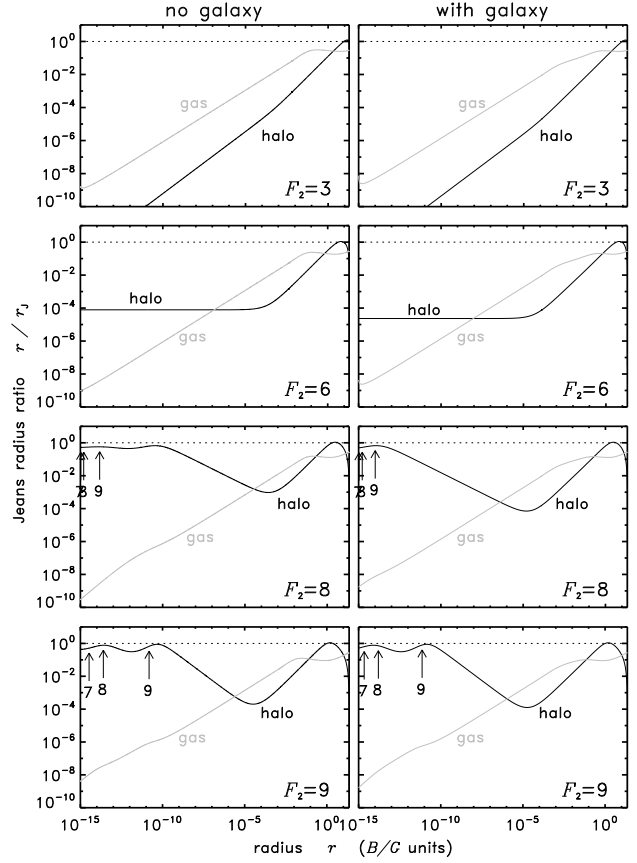


**Figure 7.** Radial profiles of Jeans stability ratio  $r_J/r$  for some minimal  $m_*$  cluster solutions in haloes with various  $F_2$  values (annotated) and total baryon fraction  $\approx 0.16$ . The dotted line shows the margin for instability. Grey curves depict the gas profile; black curves depict the dark matter. In the left-hand column, the model contains gas and dark matter only. In the right-hand column, a cD galaxy is also included ( $M_\star = 1.8 \times 10^{11} m_\odot$ ). Numbered arrows mark the radii that contain  $10^7, 10^8$  and  $10^9 m_\odot$  of dark matter.

$6 \lesssim F_2 < 10$ . The presence of a cD galaxy does not significantly modify the structures of the outer halo fringe, nor the inner core of the DM. Also it does not affect the mass spike surrounding the central object.

(iv) Stationarity of the cluster demands a positive minimal central point-mass regardless of the cD galaxy or its AGN. The range of the observed masses of SMBH in galaxies suggests that  $7 \lesssim F_2 < 10$ . The presence of a cD galaxy loosens the lower limit on realistic  $F_2$  values, but not greatly. AGN distributed heating lowers the  $m_*$  limit, when the dark matter particles have large degrees of freedom (e.g.  $F_2 = 8$ ). The dark haloes of these clusters have large heat capacities. The AGN effect upon  $m_*$  is insignificant when  $F_2$  is small (e.g.  $F_2 = 3$ ).

(v) The value of  $m_*$  can be affected by how the AGN power is spatially distributed in the intracluster gas. If  $F_2$  is large, the minimum values for the  $m_*$  limit are smaller for more evenly distributed AGN heating. If  $F_2$  is small or the halo has NFW form, the radial index of the heating does not affect  $m_*$  significantly.

(vi) The temperature variation within the ICM ( $T_{\max}/T_{\min}$ ) is maximal when  $m_*$  is minimal. Intro-



ducing the cD galaxy shrinks this ratio by a factor  $\sim 3$ . A sufficiently large point-mass  $m_*$  reduces  $T_{\max}/T_{\min}$  to the observed range ( $\lesssim 5$ ). For large  $F_2$  haloes these  $m_*$  values are consistent with real SMBH; for  $F_2 = 3$  or NFW haloes an ultramassive object is required.

(vii) The presence of a cD galaxy does not significantly affect the stability of the inner gas profile, and the inner dark halo remains prone to gravitational collapse in spite of the presence of a cD galaxy. Thus, a central SMBH can still condense or feed in dark gulps.

## ACKNOWLEDGEMENTS

This research has made use of NASA's Astrophysics Data System.

## REFERENCES

- Ackerman L., Buckley M. R., Carroll S. M., Kamionkowski M., 2009, *Phys. Rev. D*, 79, 023519
- Agnello A., Evans N. W., 2012, *ApJ*, 754, L39
- Ahn K., Shapiro P. R., 2005, *MNRAS*, 363, 1092
- Alves D. S. M., Behbahani S. R., Schuster P., Wacker J. G., 2010, *Physics Letters B*, 692, 323
- Amorisco N. C., Evans N. W., 2012, *MNRAS*, 419, 184
- Arabadjis J. S., Bautz M. W., Garmire G. P., 2002, *ApJ*, 572, 66
- Arbey A., 2006, *Phys. Rev. D*, 74, 043516
- Arbey A., Lesgourgues J., Salati P., 2003, *Phys. Rev. D*, 68, 023511
- Athreya R. M., Mellier Y., van Waerbeke L., Pelló R., Fort B., Dantel-Fort M., 2002, *A&A*, 384, 743
- Babul A., Sharma P., Reynolds C. S., 2013, *ApJ*, 768, 11
- Baker J. G., Centrella J., Choi D.-I., Koppitz M., van Meter J. R., Miller M. C., 2006, *ApJ*, 653, L93
- Bauer F. E., Fabian A. C., Sanders J. S., Allen S. W., Johnstone R. M., 2005, *MNRAS*, 359, 1481
- Binney J., Gerhard O., Silk J., 2001, *MNRAS*, 321, 471
- Birzan L., Rafferty D. A., McNamara B. R., Wise M. W., Nulsen P. E. J., 2004, *ApJ*, 607, 800
- Blumenthal G. R., Faber S. M., Flores R., Primack J. R., 1986, *ApJ*, 301, 27
- Böhmer C. G., Harko T., 2007, *JCAP*, 6, 25
- Böhringer H. et al., 2001, *A&A*, 365, L181
- Bolton A. S., Treu T., Koopmans L. V. E., Gavazzi R., Moustakas L. A., Burles S., Schlegel D. J., Wayth R., 2008, *ApJ*, 684, 248
- Bonamente M., Landry D., Maughan B., Giles P., Joy M., Nevalainen J., 2013, *MNRAS*, 428, 2812
- Bondi H., 1952, *MNRAS*, 112, 195
- Boylan-Kolchin M., Bullock J. S., Kaplinghat M., 2011, *MNRAS*, 415, L40
- Boylan-Kolchin M., Bullock J. S., Kaplinghat M., 2012, *MNRAS*, 422, 1203
- Brighenti F., Mathews W. G., 2003, *ApJ*, 587, 580
- Broadhurst T., Takada M., Umetsu K., Kong X., Arimoto N., Chiba M., Futamase T., 2005, *ApJ*, 619, L143
- Brüggen M., Kaiser C. R., 2001, *MNRAS*, 325, 676
- Bulbul G. E., Smith R. K., Foster A., Cottam J., Loewenstein M., Mushotzky R., Shafer R., 2012, *ApJ*, 747, 32
- Buote D. A., Lewis A. D., 2004, *ApJ*, 604, 116
- Burkert A., 1995, *ApJ*, 447, L25
- Campanelli M., Lousto C., Zlochower Y., Merritt D., 2007a, *ApJ*, 659, L5
- Campanelli M., Lousto C. O., Zlochower Y., Merritt D., 2007b, *Physical Review Letters*, 98, 231102
- Cappellari M., Neumayer N., Reunanen J., van der Werf P. P., de Zeeuw P. T., Rix H.-W., 2009, *MNRAS*, 394, 660
- Chandrasekhar S., 1939, *An introduction to the study of stellar structure*. Univ. Chicago Press, Chicago, IL
- Chavanis P.-H., Delfini L., 2011, *Phys. Rev. D*, 84, 043532
- Chung S. M., Gonzalez A. H., Clowe D., Zaritsky D., Markevitch M., Jones C., 2009, *ApJ*, 691, 963
- Churazov E., Brügggen M., Kaiser C. R., Böhringer H., Forman W., 2001, *ApJ*, 554, 261
- Ciotti L., Bertin G., 1999, *A&A*, 352, 447
- Clowe D., Bradač M., Gonzalez A. H., Markevitch M., Randall S. W., Jones C., Zaritsky D., 2006, *ApJ*, 648, L109
- Conroy C., Ostriker J. P., 2008, *ApJ*, 681, 151
- Cowie L. L., Binney J., 1977, *ApJ*, 215, 723
- Dahle H., Hannestad S., Sommer-Larsen J., 2003, *ApJ*, 588, L73
- David L. P., Nulsen P. E. J., McNamara B. R., Forman W., Jones C., Ponman T., Robertson B., Wise M., 2001, *ApJ*, 557, 546
- de Blok W. J. G., 2005, *ApJ*, 634, 227
- de Blok W. J. G., 2010, *Advances in Astronomy*, 2010
- de Vaucouleurs G., 1948, *Annales d'Astrophysique*, 11, 247
- de Vaucouleurs G., 1953, *MNRAS*, 113, 134
- Diego J. M., Sandvik H. B., Protopapas P., Tegmark M., Benítez N., Broadhurst T., 2005, *MNRAS*, 362, 1247
- Donahue M., Voit G. M., 2004, in *Clusters of Galaxies: Probes of Cosmological Structure and Galaxy Evolution*, Mulchaey J. S., Dressler A., Oemler A., eds., p. 143
- D'Onghia E., Lake G., 2004, *ApJ*, 612, 628
- Dubinski J., Carlberg R. G., 1991, *ApJ*, 378, 496
- Duffy A. R., Schaye J., Kay S. T., Dalla Vecchia C., 2008, *MNRAS*, 390, L64
- Dunn R. J. H., Fabian A. C., Sanders J. S., 2006, *MNRAS*, 366, 758
- Dunn R. J. H., Fabian A. C., Taylor G. B., 2005, *MNRAS*, 364, 1343
- Dursi L. J., 2007, *ApJ*, 670, 221
- Eckert D., Molendi S., Vazza F., Ettori S., Paltani S., 2013, *A&A*, 551, A22
- Eddington A. S., 1918, *ApJ*, 48, 205
- Emden R., 1907, *Gaskugeln*. Verlag B. G. Teubner, Leipzig, Berlin
- Ettori S., Fabian A. C., Allen S. W., Johnstone R. M., 2002, *MNRAS*, 331, 635
- Fabian A. C., Nulsen P. E. J., 1977, *MNRAS*, 180, 479
- Fan X. et al., 2004, *AJ*, 128, 515
- Ferreras I., Saha P., Williams L. L. R., 2005, *ApJ*, 623, L5
- Firmani C., D'Onghia E., Avila-Reese V., Chincarini G., Hernández X., 2000, *MNRAS*, 315, L29
- Flores R. A., Primack J. R., 1994, *ApJ*, 427, L1
- Frederiksen T. F., Hansen S. H., Host O., Roncadelli M., 2009, *ApJ*, 700, 1603
- Fujita Y. et al., 2008, *PASJ*, 60, 1133
- Fujita Y., Ohira Y., 2011, *ApJ*, 738, 182
- Fujita Y., Suzuki T. K., 2005, *ApJ*, 630, L1

- Garrison-Kimmel S., Rocha M., Boylan-Kolchin M., Bullock J. S., Lally J., 2013, *MNRAS*, 433, 3539
- Gavazzi R., 2005, *A&A*, 443, 793
- Gebhardt K., Adams J., Richstone D., Lauer T. R., Faber S. M., Gültekin K., Murphy J., Tremaine S., 2011, *ApJ*, 729, 119
- Gentile G., Salucci P., Klein U., Vergani D., Kalberla P., 2004, *MNRAS*, 351, 903
- Gilmore G., Wilkinson M. I., Wyse R. F. G., Kleyna J. T., Koch A., Evans N. W., Grebel E. K., 2007, *ApJ*, 663, 948
- Gnedin O. Y., Primack J. R., 2004, *Physical Review Letters*, 93, 061302
- Gnedin O. Y., Zhao H., 2002, *MNRAS*, 333, 299
- Goerdt T., Moore B., Read J. I., Stadel J., Zemp M., 2006, *MNRAS*, 368, 1073
- Gondolo P., Silk J., 1999, *Physical Review Letters*, 83, 1719
- Governato F. et al., 2010, *Nature*, 463, 203
- Graham A. W., Onken C. A., Athanassoula E., Combes F., 2011, *MNRAS*, 412, 2211
- Gültekin K. et al., 2009, *ApJ*, 698, 198
- Haiman Z., 2004, *ApJ*, 613, 36
- Hairer E., Nørsett S. P., Wanner G., 2008, *Solving Ordinary Differential Equations. I. Nonstiff Problems*, 2nd edn. Springer-Verlag, Berlin
- Halkola A., Hildebrandt H., Schrabback T., Lombardi M., Bradač M., Erben T., Schneider P., Wuttke D., 2008, *A&A*, 481, 65
- Halkola A., Seitz S., Pannella M., 2006, *MNRAS*, 372, 1425
- Harko T., 2011, *MNRAS*, 413, 3095
- Harko T., Lobo F. S. N., 2011, *Phys. Rev. D*, 83, 124051
- Harko T., Lobo F. S. N., 2012, *Astroparticle Physics*, 35, 547
- Houghton R. C. W., Magorrian J., Sarzi M., Thatte N., Davies R. L., Krajnović D., 2006, *MNRAS*, 367, 2
- Huntley J. M., Saslaw W. C., 1975, *ApJ*, 199, 328
- Ichikawa K. et al., 2013, *ApJ*, 766, 90
- Ikebe Y. et al., 1997, *ApJ*, 481, 660
- Ilyin A. S., Zybin K. P., Gurevich A. V., 2004, *Soviet Journal of Experimental and Theoretical Physics*, 98, 1
- Inada N., Oguri M., Falco E. E., Broadhurst T. J., Ofek E. O., Kochanek C. S., Sharon K., Smith G. P., 2008, *PASJ*, 60, L27
- Inoue S., 2009, *MNRAS*, 397, 709
- Jardel J. R., Gebhardt K., 2012, *ApJ*, 746, 89
- Jee M. J., Mahdavi A., Hoekstra H., Babul A., Dalcanton J. J., Carroll P., Capak P., 2012, *ApJ*, 747, 96
- Johnstone R. M., Allen S. W., Fabian A. C., Sanders J. S., 2002, *MNRAS*, 336, 299
- Johnstone R. M., Fabian A. C., Edge A. C., Thomas P. A., 1992, *MNRAS*, 255, 431
- Kaastra J. S., Ferrigno C., Tamura T., Paerels F. B. S., Peterson J. R., Mittaz J. P. D., 2001, *A&A*, 365, L99
- Kaplan D. E., Krnjaic G. Z., Rehermann K. R., Wells C. M., 2010, *JCAP*, 5, 21
- Katgert P., Biviano A., Mazure A., 2004, *ApJ*, 600, 657
- Kelson D. D., Zabludoff A. I., Williams K. A., Trager S. C., Mulchaey J. S., Bolte M., 2002, *ApJ*, 576, 720
- Kirihara T., Miki Y., Mori M., 2013, *Journal of Physics Conference Series*, 454, 012012
- Kleyna J. T., Wilkinson M. I., Gilmore G., Evans N. W., 2003, *ApJ*, 588, L21
- Klypin A., Kravtsov A. V., Valenzuela O., Prada F., 1999, *ApJ*, 522, 82
- Kronawitter A., Saglia R. P., Gerhard O., Bender R., 2000, *A&AS*, 144, 53
- Kuzio de Naray R., McGaugh S. S., de Blok W. J. G., Bosma A., 2006, *ApJS*, 165, 461
- Lane J. H., 1870, *The American Journal of Science and Arts*, 2nd series, 50, 57
- Lima Neto G. B., Gerbal D., Márquez I., 1999, *MNRAS*, 309, 481
- Loeb A., Weiner N., 2011, *Physical Review Letters*, 106, 171302
- Loewenstein M., Mathews W. G., 1987, *ApJ*, 319, 614
- Loewenstein M., White, III R. E., 1999, *ApJ*, 518, 50
- Lousto C. O., Zlochower Y., 2011, *Physical Review Letters*, 107, 231102
- Lousto C. O., Zlochower Y., 2013, *Phys. Rev. D*, 87, 084027
- MacMillan J. D., Henriksen R. N., 2002, *ApJ*, 569, 83
- Mahdavi A., Hoekstra H., Babul A., Balam D. D., Capak P. L., 2007, *ApJ*, 668, 806
- Márquez I., Lima Neto G. B., Capelato H., Durret F., Gerbal D., 2000, *A&A*, 353, 873
- Mashchenko S., Couchman H. M. P., Wadsley J., 2006, *Nature*, 442, 539
- Mathews W. G., Brighenti F., 2003, *ARA&A*, 41, 191
- Matsushita K., Belsole E., Finoguenov A., Böhringer H., 2002, *A&A*, 386, 77
- McConnell N. J., Ma C.-P., Gebhardt K., Wright S. A., Murphy J. D., Lauer T. R., Graham J. R., Richstone D. O., 2011, *Nature*, 480, 215
- McConnell N. J., Ma C.-P., Murphy J. D., Gebhardt K., Lauer T. R., Graham J. R., Wright S. A., Richstone D. O., 2012, *ApJ*, 756, 179
- McNamara B. R., Nulsen P. E. J., 2007, *ARA&A*, 45, 117
- Memola E., Salucci P., Babić A., 2011, *A&A*, 534, A50+
- Merritt D., 2004, *Physical Review Letters*, 92, 201304
- Merritt D., 2010, *ArXiv e-prints*, 1001.3706
- Merritt D., Navarro J. F., Ludlow A., Jenkins A., 2005, *ApJ*, 624, L85
- Miller S. H., Ellis R. S., Newman A. B., Benson A., 2013, *ArXiv e-prints*, 1310.1079
- Molendi S., Pizzolato F., 2001, *ApJ*, 560, 194
- Moore B., 1994, *Nature*, 370, 629
- Moore B., Gelato S., Jenkins A., Pearce F. R., Quilis V., 2000, *ApJ*, 535, L21
- Moore B., Quinn T., Governato F., Stadel J., Lake G., 1999, *MNRAS*, 310, 1147
- Moretti A., Gastaldello F., Ettori S., Molendi S., 2011, *A&A*, 528, A102
- Mortlock D. J. et al., 2011, *Nature*, 474, 616
- Murphy J. D., Gebhardt K., Adams J. J., 2011, *ApJ*, 729, 129
- Nagino R., Matsushita K., 2009, *A&A*, 501, 157
- Narayan R., Medvedev M. V., 2001, *ApJ*, 562, L129
- Navarro J. F., Eke V. R., Frenk C. S., 1996, *MNRAS*, 283, L72
- Navarro J. F., Frenk C. S., White S. D. M., 1996, *ApJ*, 462, 563
- Navarro J. F. et al., 2004, *MNRAS*, 349, 1039
- Nevalainen J., Markevitch M., Forman W., 1999, *ApJ*, 526, 1
- Newman A. B., Treu T., Ellis R. S., Sand D. J., Richard

- J., Marshall P. J., Capak P., Miyazaki S., 2009, *ApJ*, 706, 1078
- Norris M. A. et al., 2012, *MNRAS*, 421, 1485
- Nulsen P. E. J., 1986, *MNRAS*, 221, 377
- Nunez D., Sussman R. A., Zavala J., Cabral-Rosetti L. G., Matos T., 2006, in *AIP Conf. Proc.*, Vol. 857, *Particles and Fields: X Mexican Workshop*, Pérez M. A., Urrutia L., Villaseqor L., eds., p. 316
- Oh S.-H., de Blok W. J. G., Walter F., Brinks E., Kennicutt R., 2008, *AJ*, 136, 2761
- O'Sullivan E., Vrtilek J. M., Harris D. E., Ponman T. J., 2007, *ApJ*, 658, 299
- O'Sullivan E., Worrall D. M., Birkinshaw M., Trinchieri G., Wolter A., Zezas A., Giacintucci S., 2011, *MNRAS*, 416, 2916
- Peñarrubia J., Pontzen A., Walker M. G., Kopesov S. E., 2012, *ApJ*, 759, L42
- Peebles P. J. E., 2000, *ApJ*, 534, L127
- Peebles P. J. E., Nusser A., 2010, *Nature*, 465, 565
- Peirani S., Kay S., Silk J., 2008, *A&A*, 479, 123
- Peter A. H. G., Rocha M., Bullock J. S., Kaplinghat M., 2013, *MNRAS*, 430, 105
- Peterson J. R., Fabian A. C., 2006, *Phys. Rep.*, 427, 1
- Peterson J. R., Kahn S. M., Paerels F. B. S., Kaastra J. S., Tamura T., Bleeker J. A. M., Ferrigno C., Jernigan J. G., 2003, *ApJ*, 590, 207
- Peterson J. R. et al., 2001, *A&A*, 365, L104
- Plastino A. R., Plastino A., 1993, *Physics Letters A*, 174, 384
- Plummer H. C., 1911, *MNRAS*, 71, 460
- Pointecouteau E., Arnaud M., Pratt G. W., 2005, *A&A*, 435, 1
- Prince P. J., Dormand J. R., 1981, *Journal of Computational and Applied Mathematics*, 7, 67
- Prugniel P., Simien F., 1997, *A&A*, 321, 111
- Pu S. B., Saglia R. P., Fabricius M. H., Thomas J., Bender R., Han Z., 2010, *A&A*, 516, A4
- Quinlan G. D., Hernquist L., Sigurdsson S., 1995, *ApJ*, 440, 554
- Randall S. W., Markevitch M., Clowe D., Gonzalez A. H., Bradač M., 2008, *ApJ*, 679, 1173
- Reiprich T. H. et al., 2009, *A&A*, 501, 899
- Richard J., Pei L., Limousin M., Jullo E., Kneib J. P., 2009, *A&A*, 498, 37
- Richtler T., Salinas R., Misgeld I., Hilker M., Hau G. K. T., Romanowsky A. J., Schuberth Y., Spolaor M., 2011, *A&A*, 531, A119
- Ritter A., 1878, *Wiedemann Annalen*, 5, 543
- Rocha M., Peter A. H. G., Bullock J. S., Kaplinghat M., Garrison-Kimmel S., Oñorbe J., Moustakas L. A., 2013, *MNRAS*, 430, 81
- Ruszkowski M., Begelman M. C., 2002, *ApJ*, 581, 223
- Ruszkowski M., Oh S. P., 2010, *ApJ*, 713, 1332
- Rybicki G. B., Lightman A. P., 1979, *Radiative Processes in Astrophysics*. Wiley, New York
- Rzepecki J., Lombardi M., Rosati P., Bignamini A., Tozzi P., 2007, *A&A*, 471, 743
- Saha P., Read J. I., 2009, *ApJ*, 690, 154
- Sakelliou I. et al., 2002, *A&A*, 391, 903
- Salucci P., Burkert A., 2000, *ApJ*, 537, L9
- Sand D. J., Treu T., Ellis R. S., 2002, *ApJ*, 574, L129
- Sand D. J., Treu T., Ellis R. S., Smith G. P., Kneib J.-P., 2008, *ApJ*, 674, 711
- Sanders J. S., Fabian A. C., Allen S. W., Morris R. G., Graham J., Johnstone R. M., 2008, *MNRAS*, 385, 1186
- Sanders J. S., Fabian A. C., Smith R. K., Peterson J. R., 2010, *MNRAS*, 402, L11
- Sarazin C. L., 1988, X-ray emission from clusters of galaxies
- Sarazin C. L., Ashe G. A., 1989, *ApJ*, 345, 22
- Sarazin C. L., White, III R. E., 1987, *ApJ*, 320, 32
- Saxton C. J., 2013, *MNRAS*, 430, 1578
- Saxton C. J., Ferreras I., 2010, *MNRAS*, 405, 77
- Saxton C. J., Soria R., Wu K., Kuin N. P. M., 2012, *MNRAS*, 422, 1625
- Saxton C. J., Sutherland R. S., Bicknell G. V., 2001, *ApJ*, 563, 103
- Saxton C. J., Wu K., 2008, *MNRAS*, 391, 1403
- Schnittman J. D., Buonanno A., 2007, *ApJ*, 662, L63
- Sellwood J. A., 2009, in *IAU Symposium*, Vol. 254, *IAU Symposium*, J. Andersen, J. Bland-Hawthorn, & B. Nordström, ed., pp. 73–84
- Sérsic J. L., 1968, *Atlas de galaxias australes*. Cordoba, Argentina: Observatorio Astronomico, 1968
- Shields G. A., Bonning E. W., 2013, *ApJ*, 772, L5
- Simionescu A. et al., 2011, *Science*, 331, 1576
- Slepian Z., Goodman J., 2012, *MNRAS*, 427, 839
- Soltan A., 1982, *MNRAS*, 200, 115
- Spergel D. N., Steinhardt P. J., 2000, *Physical Review Letters*, 84, 3760
- Stewart G. C., Fabian A. C., Nulsen P. E. J., Canizares C. R., 1984, *ApJ*, 278, 536
- Sun M., Voit G. M., Donahue M., Jones C., Forman W., Vikhlinin A., 2009, *ApJ*, 693, 1142
- Takahashi I. et al., 2009, *ApJ*, 701, 377
- Tamura T. et al., 2001, *A&A*, 365, L87
- Thomas J., Saglia R. P., Bender R., Thomas D., Gebhardt K., Magorrian J., Corsini E. M., Wegner G., 2005, *MNRAS*, 360, 1355
- Thomas J., Saglia R. P., Bender R., Thomas D., Gebhardt K., Magorrian J., Corsini E. M., Wegner G., 2007, *MNRAS*, 382, 657
- Tikhonov A. V., Klypin A., 2009, *MNRAS*, 395, 1915
- Tsallis C., 1988, *Journal of Statistical Physics*, 52, 479
- Ullio P., Zhao H., Kamionkowski M., 2001, *Phys. Rev. D*, 64, 043504
- Umetsu K., Broadhurst T., 2008, *ApJ*, 684, 177
- Urban O., Werner N., Simionescu A., Allen S. W., Böhringer H., 2011, *MNRAS*, 414, 2101
- Vasiliev E., Zelnikov M., 2008, *Phys. Rev. D*, 78, 083506
- Vedder P. W., Trester J. J., Canizares C. R., 1988, *ApJ*, 332, 725
- Vernaleo J. C., Reynolds C. S., 2006, *ApJ*, 645, 83
- Viala Y., Horedt G. P., 1974a, *A&AS*, 16, 173
- Viala Y. P., Horedt G., 1974b, *A&A*, 33, 195
- Vignat C., Plastino A., Plastino A. R., 2011, *Phys. A*, 390, 2491
- Vikhlinin A., Kravtsov A., Forman W., Jones C., Markevitch M., Murray S. S., Van Speybroeck L., 2006, *ApJ*, 640, 691
- Vogelsberger M., Zavala J., Loeb A., 2012, *MNRAS*, 423, 3740
- Voigt L. M., Fabian A. C., 2004, *MNRAS*, 347, 1130
- Voigt L. M., Fabian A. C., 2006, *MNRAS*, 368, 518



- Walker M. G., Peñarrubia J., 2011, *ApJ*, 742, 20
- Weijmans A.-M., Krajinović D., van de Ven G., Oosterloo T. A., Morganti R., de Zeeuw P. T., 2008, *MNRAS*, 383, 1343
- Werner N., de Plaa J., Kaastra J. S., Vink J., Bleeker J. A. M., Tamura T., Peterson J. R., Verbunt F., 2006, *A&A*, 449, 475
- White, III R. E., Chevalier R. A., 1984, *ApJ*, 280, 561
- Williams L. L. R., Saha P., 2011, *MNRAS*, 415, 448
- Xue Y.-J., Böhringer H., Matsushita K., 2004, *A&A*, 420, 833
- Yoshida N., Springel V., White S. D. M., Tormen G., 2000, *ApJ*, 544, L87
- Zavala J., Núñez D., Sussman R. A., Cabral-Rosetti L. G., Matos T., 2006, *Journal of Cosmology and Astro-Particle Physics*, 6, 8
- Zelnikov M. I., Vasiliev E. A., 2005, *Soviet Journal of Experimental and Theoretical Physics Letters*, 81, 85
- Zhang Y.-Y., Böhringer H., Finoguenov A., Ikebe Y., Matsushita K., Schuecker P., Guzzo L., Collins C. A., 2006, *A&A*, 456, 55
- Zitrin A., Broadhurst T., 2009, *ApJ*, 703, L132

## APPENDIX A: ALTERNATIVE HALO PROFILES

Our main results focused on cluster models with a large  $F_2$  halo, because these give  $m_*$  mass limits consistent with realistic SMBH. Here, we will briefly compare the benchmark  $F_2 = 8$  models to the results for point-like ‘monatomic’ SIDM ( $F_2 = 3$ ) and the popular ‘NFW’ profile (Navarro, Frenk & White 1996). ‘Monatomic’ SIDM ( $F_2 = 3$ ) can represent conditions similar to the most often studied SIDM theories (e.g. Moore et al. 2000; Ahn & Shapiro 2005; Peter et al. 2013; Rocha et al. 2013) but with stronger scattering. The NFW profile could describe the cuspy or small-cored haloes of collisionless DM theories, or forms of SIDM that are so weakly collisional that the core fails to grow to the full size attainable in an ideal Lane–Emden sphere. The NFW radial density profile is

$$\rho_{\text{nfw}} = \frac{\rho_0 R_s^3}{r(R_s + r)^2}. \quad (\text{A1})$$

For the NFW modelling, we select a representative concentration  $c = R_v/R_s \approx 3.471$  from the mass–concentration relation of Duffy et al. (2008). The corresponding ‘virial radius’ and scale radius are  $R_v = 5.897U_x \approx 1.45\text{Mpc}$  and  $R_s = 1.699U_x \approx 0.42\text{Mpc}$ . The halo is truncated at the chosen radius  $R$ . For each trial choice of the outer Mach number ( $\mathcal{M}_R$ ) and temperature ( $T_R$ ), the NFW density normalization ( $\rho_0$ ) is varied until the total mass of the system (gas + stars + halo + SMBH) matches our standard value ( $40U_m$ ). This density scale replaces the role of  $s_2$  as a computational search parameter in the cluster configuration-space.

In all cases, the gas inflow from external cosmic background is set to our standard  $T_R = 1\text{keV}$  temperature and  $\dot{m} = 10 m_\odot \text{yr}^{-1}$ . Under the effect a cD galaxy and AGN heating, the global mass-radius relations and the baryon fraction versus  $R$  relations of the  $F_2 = 3$  and NFW models are qualitatively similar to those of  $F_2 = 8$ , and need not be shown here.

In the absence of a cD galaxy, all cosmologically reasonable baryon fractions imply a minimum  $m_* \gtrsim 10^{10} m_\odot$  for  $F_2 = 3$ , and  $m_* \gtrsim 8 \times 10^9 m_\odot$  for NFW models (dashed lines in Figs A1 and A2 respectively). The gravitational presence of the standard cD galaxy lowers these limits to  $m_* \approx 4 \times 10^9 m_\odot$ . The cluster radius  $R$  has negligible effect on these limits. The power and functional form of the AGN heating has little further effect on  $m_*$  limits for  $F_2 = 3$  and NFW models: e.g. the  $10^{-4}U_L$ ,  $10^{-3}U_L$  and  $10^{-2}U_L$  power curves are almost inseparable in the panels of Figs A1 and A2. For the NFW cases, raising the AGN output from zero up to  $10^{-2}U_L$  makes a few percent difference in  $m_*$ , though not enough to be visible on the scale of Fig. A2. For  $F_2 = 3$  (Fig. A1) the difference is much smaller. In summary, for  $F_2 = 8$ ,  $F_2 = 3$  and NFW scenarios alike, we find that the  $m_*$  limit is influenced more by the cD galaxy potential (at kpc radii) than by any AGN heating, but the AGN effects are greater for  $F_2 = 8$  than the alternative haloes.

Fig. A3 is analogous to Fig. 6: showing the ICM temperature range  $T_{\text{max}}/T_{\text{min}}$  attainable in a set of self-consistent solutions of the  $F_2 = 3$  clusters of outer radius  $R = 16U_x \approx 3.93\text{Mpc}$  and different central masses above the minimum  $m_*$ . Fig. A4 shows the corresponding NFW models. The curves depict cases without cD galaxy (dashed), with an inactive cD galaxy (grey), and various heating functions at high power ( $10^{-2}U_L$ , annotated by  $\nu$ ). Each scenario appears as two joined curves: they correspond to the ‘too fast’ and ‘too cold’ borders bounding the physically allowed zone in the configuration space. At the minimum  $m_*$  extreme, the greatest  $T_{\text{max}}/T_{\text{min}} \lesssim 35$  for  $F_2 = 3$ , and  $T_{\text{max}}/T_{\text{min}} \lesssim 14$  for NFW background. We previously saw that AGN heating in  $F_2 = 8$  clusters has little effect on the temperature ratio of the ICM. Now in the  $F_2 = 3$  and NFW models it appears that AGN heating *increases*  $T_{\text{max}}/T_{\text{min}}$  relative to the case of an inactive galaxy. This effect is weaker for more concentrated heating (larger  $\nu$ ). The gas temperature range only agrees with observed values of large clusters ( $2.5 \lesssim T_{\text{max}}/T_{\text{min}} \lesssim 4.5$ , the grey shaded band) if the central point-mass is comparable to the combined mass of the stars,  $m_* \gtrsim M_\star/2$ . To achieve a realistic  $T_{\text{max}}/T_{\text{min}}$ , the  $F_2 = 8$  halo model only requires a central object of a few  $10^8 m_\odot$ . On these grounds, we re-emphasize that the large- $F_2$  regime is more plausible than NFW or  $F_2 = 3$  models. We would encourage astroparticle theorists to focus on candidate particles and fields that would naturally provide forms of dark matter with properties in the interval of  $7 \lesssim F_2 < 10$ .

## APPENDIX B: X-RAY TEMPERATURE FITS

The formulation presented in this work can also be used in parameter extractions from observational data, thus enabling comparisons between models and observations. Here, we show a simple conceptual demonstration in which temperature profiles derived from X-ray observations are fitted by the cluster model discussed in this paper. We extract projected gas temperature profiles (and error bars) from the data files in an online version of Vikhlinin et al. (2006). For the purpose of this exercise, we will treat the two-dimensional projected temperature profile as representative of the three-dimensional spherical profile.

Assuming  $F_2 = 8$  and our standard outer boundary con-



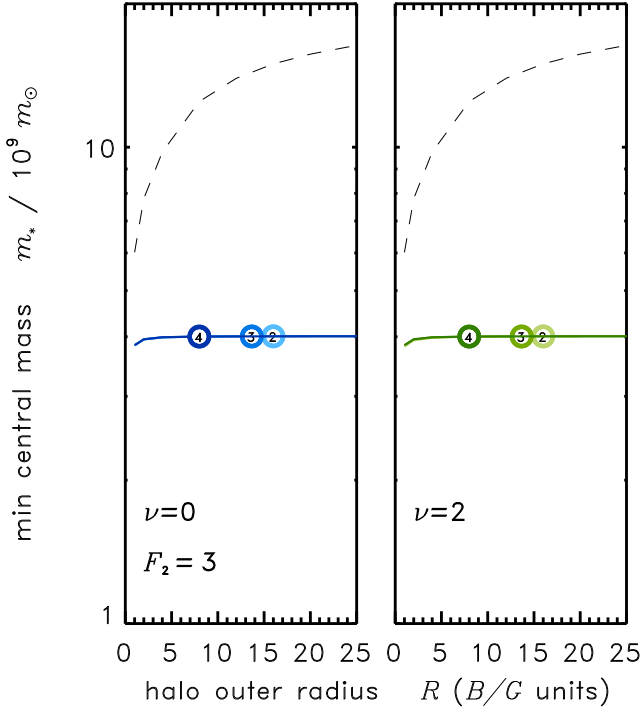


**Figure A1.** Minimum central mass ( $m_*$ ) for clusters with  $F_2 = 3$  and various outer radii. Left-hand panel shows the effect of spatially uniform heating ( $\nu = 0$ ), and right-hand panel shows concentrated heating with  $\nu = 2$ . AGN power (annotated as in Fig. 2 and 3) makes little difference to the limiting  $m_*$ . The dashed curve shows results without a cD galaxy.

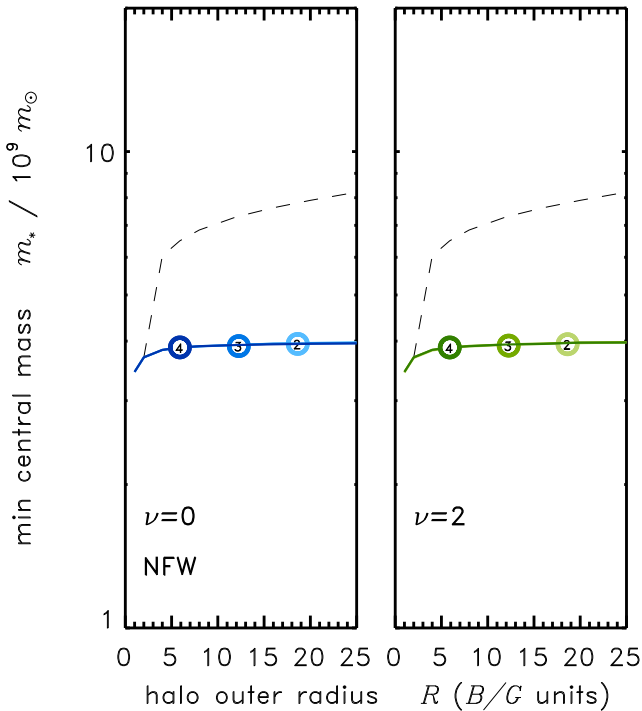


**Figure A2.** Minimum central mass ( $m_*$ ) versus cluster radius as in Fig. A1 but with a NFW halo profile. The  $m_*$  show slightly more variation with  $R$  and AGN power than the  $F_2 = 3$  models, but less than for the preferred  $F_2 = 8$  scenario.

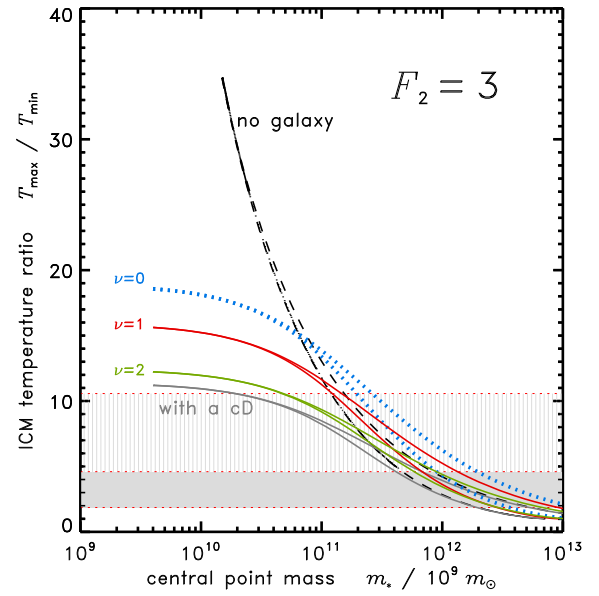


**Figure A3.** The  $(T_{\max}/T_{\min})$  ratio of the ICM for cluster models with radius  $R = 16U_x \approx 3.93$  Mpc and  $F_2 = 3$  polytropic halo. As in Fig. 6, the grey shaded area is the range of ratios observed in cooling flow clusters, and the striped region includes the Centaurus A group.

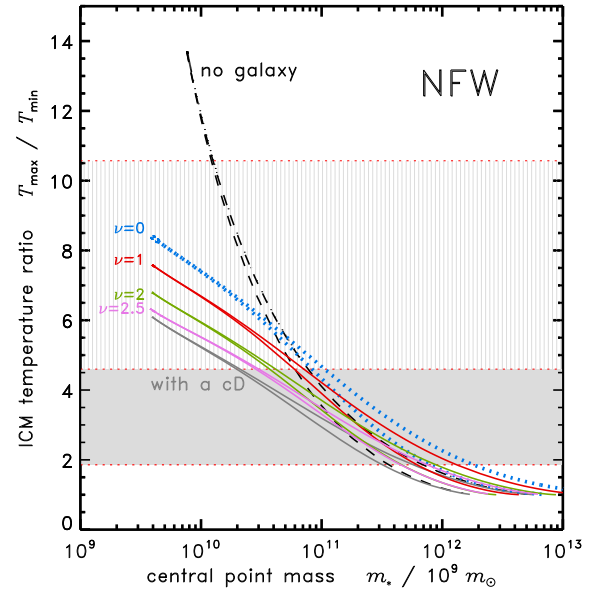


**Figure A4.** The  $(T_{\max}/T_{\min})$  ratio of the intracluster gas for cluster models equivalent to Fig. 6 and Fig. A3, but with ‘NFW’ dark halo profiles.

ditions, we vary presence/absence of the cD galaxy, and the halo radius  $R = 4, 6, 8, 10, 12, 14, 16U_x$ . The baryon fraction is not controlled in these tests; we allow whatever values of  $M_1$  and  $M_2$  happen to emerge from  $m_*$ -minimization. We gather the cluster solutions at different  $\mathcal{M}_R$  just along the acceptable side of the ‘too fast’ border in configuration

space. For each model, we compute the  $\chi^2$  best fit to the projected  $T(r)$  data, allowing a linear auto-normalization process to obtain the best-fitting mass scale. In effect, the fit has one continuous fitting variable ( $\mathcal{M}_R$ , since optimization of  $s_2$  is implied) and coarse trial values for  $R$ .

Despite this inflexibility, the reduced  $\chi^2/\text{d.o.f.} \approx 2$ . We might expect tighter fits (and perhaps too much parameter degeneracy) if the baryon fraction,  $\dot{m}$ ,  $T_R$  and  $R$  were all varied continually and independently of  $\mathcal{M}_R$  and the mass normalization. A383 is the most massive of the three example systems fitted, with  $R = 8U_x \approx 2.0\text{Mpc}$ , and auto-normalization giving mass of  $M = 2.2 \times 10^{14} m_\odot$  and inflow  $\dot{m} = 5.0 m_\odot \text{ yr}^{-1}$  ( $\chi^2 = 21.9$  for 9 bins). For A1991,  $R = 6U_x \approx 1.5\text{Mpc}$ ,  $M = 8.2 \times 10^{13} m_\odot$  and  $\dot{m} = 1.1 m_\odot \text{ yr}^{-1}$  ( $\chi^2 = 25.3$  for 10 bins). For USGC S152,  $R = 4U_x \approx 0.98\text{Mpc}$ ,  $M = 1.3 \times 10^{13} m_\odot$  and  $\dot{m} = 0.068 m_\odot \text{ yr}^{-1}$  ( $\chi^2 = 15.5$  for 9 bins). Note that the value of  $\dot{m}^3/M^2$  is implicitly fixed constant. Unlike the original semi-parametric modelling by Vikhlinin et al. (2006), we do not need to omit any of the innermost points. This inclusion enables our fits with a DM core rather than cusp. The central rise in temperature (in some objects, e.g. in USGC S152) emerges naturally in our formulation. The uphill and downhill slopes around the temperature dip and peak also turn out to be similar to those appearing in nature.

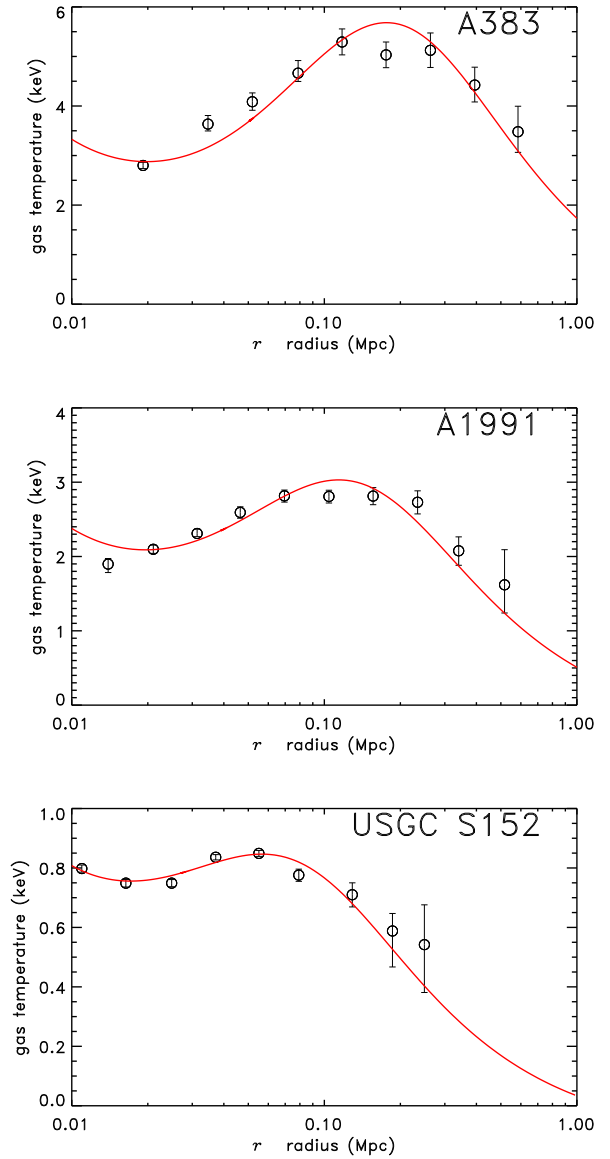


**Figure B1.** Cluster model fits to three of the cluster temperature profiles from Vikhlinin et al. (2006). The X-ray derived temperatures are projected, but the model profiles are three-dimensional.